Radial Distributions of Various Stellar Populations and the Evolution of the Globular Cluster 47 Tucanae

by

Javiera Fernanda Parada Torres

A THESIS SUBMITTED IN PARTIAL FULFILLMENT
OF THE REQUIREMENTS FOR THE DEGREE OF

MASTER OF SCIENCE

in

THE FACULTY OF GRADUATE AND POSTDOCTORAL STUDIES
(Astronomy)

THE UNIVERSITY OF BRITISH COLUMBIA
(Vancouver)

January 2016

Abstract

Blue stragglers (BSS) are stars whose position in the Color-Magnitude Diagram (CMD) places them above the main sequence turn-off point in a given cluster. Three possible origins have been proposed: stellar collisions, evolution of binary systems, and evolution of hierarchical triples. Using data from the core of 47 Tuc in the ultraviolet (UV), we have identified various stellar populations in the CMD, and used their radial distributions to study the evolution and origin of BSS. When we separate the BSS in two samples divided by their magnitude, we find that the bright BSS show a much more centrally concentrated radial distribution and higher mass estimates, suggesting an origin involving triple or multiple stellar systems. In contrast, the faint BSS are less concentrated, with a radial distribution similar to the main sequence (MS) binaries pointing to this populations as their progenitors. A sample of evolved BSS was found on the UV CMD, this put together with available photometric data and MESA evolutionary models resulted in time scales and number of observed and expected stars agreeing nicely with the BSS having a post-MS evolution comparable to that of a normal star of the same mass and a MS BSS lifetime of about 200-300 Myr. We also find that the extra population of the asymptotic giant branch (AGB) stars in 47 Tuc is due to evolved BSS, with the bulk of the contamination being in the red giant branch bump of the BSS that, according to our models, falls in the same magnitude and color range as the observed AGB bump.

Preface

The data reduction, briefly explained in Chapter 2, that led to the photometry files in the ultraviolet filters used in this thesis, was carried out by Jason Kalirai following the procedures described in Kalirai et al. (2012). For the ACS data, the photometry file is of public domain and can be obtain at http://www.astro.ufl.edu/ata/publichstgc/databases.html.

The same evolutionary models and isochrones presented in this thesis were used in Heyl et al. (2015a) of which I am a co-author. The completeness rates have also been previously published in Heyl et al. (2015b) of which I am also a co-author.

Everything bother than the above is an original, unpublished, independent work by the author, J. Parada.

Table of Contents

List of Tables

List of Figures

Glossary

ACS Advanced Camera for Surveys

AGB Asymptotic Giant Branch

b-b Binary-Binary (encounters)

bBSS Bright Blue Stragglers

BSS Blue Stragglers

CMD Colour-Magnitude Diagram

CNO Carbon-Nitrogen-Oxygen (cycle)

fBSS Faint Blue Stragglers

GC Globular Cluster

HB Horizontal Branch

HST Hubble Space Telescope

KS-test Kolmogorov-Smirnov test

MAST Barbara A. Mikulski Archive for Space Telescopes

MESA Module for Experiments in Stellar Astrophysics

MS Main Sequence

MT Mass Transfer

pp Proton-Proton (chain)

PSF Point-Spread-Function

RGB Red Giant Branch

r_c	Core Radius
r_h	Half-Light Radius
s-b	Single-Binary (encounters)
SGB	Sub-Giant Branch
SMC	Small Magellanic Cloud
s-s	Single-Single (encounters)
t_{cross}	Crossing Time
t_{evol}	Dynamical Evolution Time
TO	Turn Off
t_{relax}	Relaxation Time
UV	Ultraviolet
WD	White Dwarf
WFC3	Wide Field Camera 3
ZAMS	Zero Age MS

Acknowledgements

I would like to gratefully acknowledge the help and guidance from my supervisors Dr. Harvey Richer and Dr. Jeremy Heyl throughout this project.

I would like to thank to Dr. Jason Kalirai for sharing his data reduction and photometry knowledge, key to this research.

I would also like to express my gratitude to Dr. Patricio Rojo, who had no obligation but took the time to teach me scientific skills that I had no idea were needed for graduate school.

Finally and most importantly, I would like to thank my family, especially my parents, for their unconditional support (emotional and financial), motivation and love, not only now but throughout my life. And my friends, life would be boring without them.

Chapter 1

Introduction

Globular star clusters (GC) are roughly spherical groups of stars thought to be composed of a simple stellar population, having all the stars born at the same time setting a perfect laboratory for the study of stellar evolution. With the development of astronomical instrumentation, scientists have been able to study GC in more detail, exposing the presence of different anomalous stellar populations. An important example of such stars are blue stragglers (BSS). First discovered by Sandage (1953) in the GC M3, BSS were described as an extension of the main sequence (MS) defying normal stellar evolution within a cluster (see section 1.1). How these stars are formed in GC and where do they go after they leave their MS stage has been a constant debate.

With a large sample of 157 GC in the galaxy (Harris, 1996), these agglomeration of stars are one of the most widely studied systems in astronomy due to their versatility. Not only are they a good place to study the evolution of stars and dynamics of stellar systems, but they also give us information about the structure, chemical composition and dynamical history of the Milky Way. A good example of a well studied system is NGC 104 (47 Tucanae). Visible from the southern hemisphere, 47 Tuc is the second largest and brightest GC in the sky. Located at ~ 4.7 kiloparsecs from the Sun (Woodley et al., 2012), 47 Tuc is home to 2 million stars. Although 47 Tuc has been the target of many investigations, this thesis is the first time such a big portion of the core of the cluster has been observed with ultraviolet filters, allowing us to go deeper into the most dense region of this system (more details of the observations procedure will be given in Chapter 2).

One way to study the evolution of GCs and the stars in it, is to use photometric data, which can be used to create a colour-magnitude diagram (CMD) using the measured magnitudes and also radial distributions using the positions for each star. The CMD will allow us to separate the stars of the cluster into different stellar evolutionary stages while the radial distributions will tell us about the dynamics of the system.

We will begin with a brief explanation of stellar evolution and how CMDs help us trace the different populations in a GC followed by a section on the dynamics of these systems. The last section of the introduction will give a detailed summary of the historic and current results on the formation and evolution of BSS relevant to this investigation.

1.1 Colour-Magnitude Diagrams and Stellar Evolution

A Colour-Magnitude Diagram is a scatter plot showing, as the name suggest, the relationship between apparent magnitude (luminosity) and color (effective temperature) of stars. The apparent magnitude of a star depends on the distance of the star with respect to Earth, in this case we can use such a plot because the stars of GCs are considered to be all at the same distance from Earth.

To understand the CMD, we need to first understand stellar evolution. To keep things connected, we will trace the evolution of a one solar mass ($1M_{\odot}$) star in terms of a MESA (Modules for Experiments in Stellar Astrophysics; Paxton et al. 2011, 2013, 2015) model placed in CMD space (Figure 1.1) and go through the different stages. We chose this particular mass as it covers all the evolutionary stages seen on the CMD of 47 Tucanae (and some extra stages that due to the short time for which they exist is almost impossible to see on the CMD of a GC). There are though some differences in the evolution of stars with lower and higher masses than $1M_{\odot}$ and they will be mentioned when the differences become important. We will leave aside the formulas that explain the physical processes going on inside the stars and focus mostly on a description. This section is intended as an introduction to understand what is going on in each stage that will later be used to trace the evolution of the cluster and not as an introduction to stellar astrophysics.

1.1.1 The Evolution of a Solar Mass Star

Star formation begins in the interstellar medium when a molecular cloud becomes unstable to gravitational collapse and a protostar is formed. The initial stages of stellar formation, and how we get to a protostar still generate some debate. The end of this rapid contraction phase is marked by the beginning of the Hayashi track (marked as (1) on Figure 1.1). The star is now on its way to the MS, the collapse rate slows down and the star becomes fully convective. Contraction continues as the protostar moves down the Hayashi track; luminosity and stellar radius decrease until it develops a radiative core. At this point the protostar enters the Henyey track (2), here it becomes hotter until contraction ends and the core is hot enough for the protostar to begin hydrogen fusion (3) which marks the birth of the star as it reaches the zero age MS (ZAMS) (Collins, 1989).

The MS is the longest evolutionary stage of a star, the lower the mass the more time it

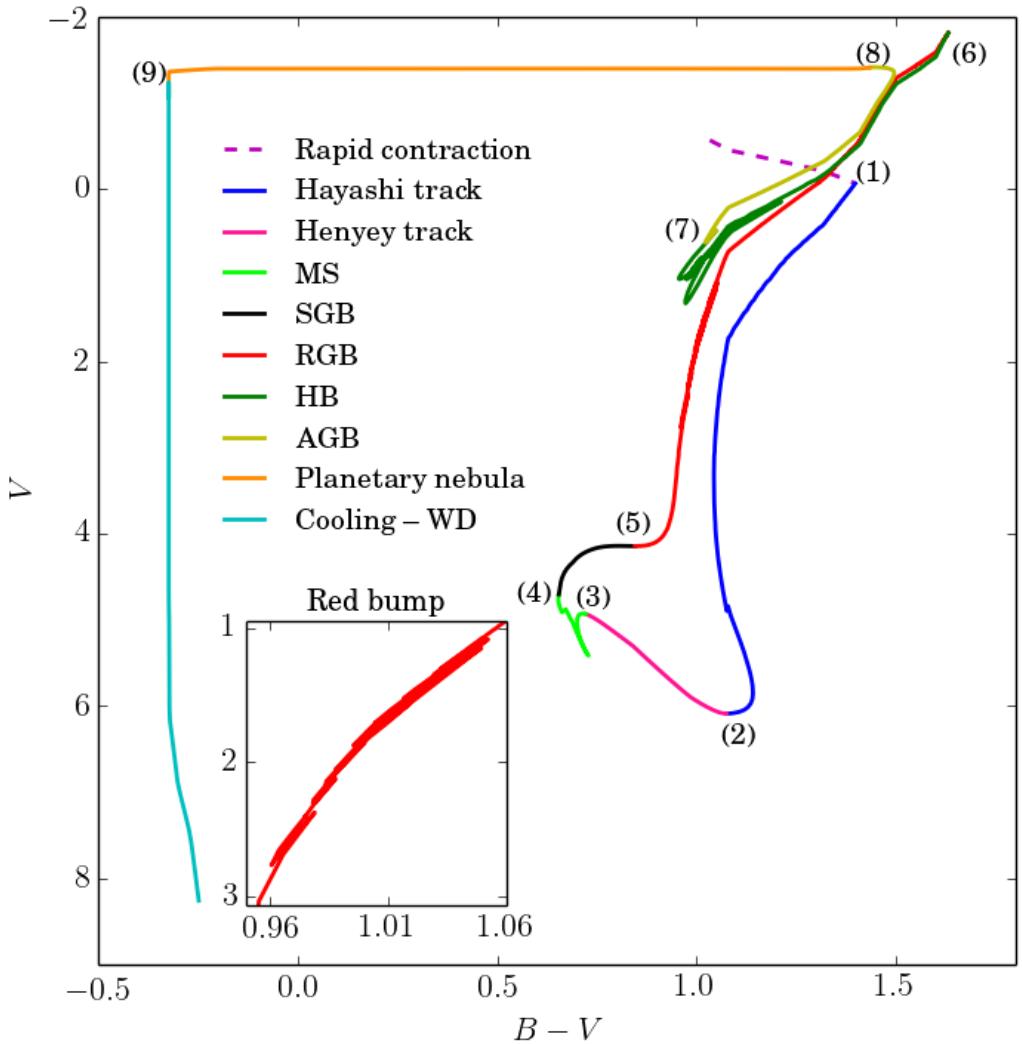

Figure 1.1: MESA evolutionary model for a $1M_\odot$ star. The model was coloured to a CMD using table 1.4 from Sparke & Gallagher (2007). The different colours along the model curve represent the different evolutionary stages of the star while the numbers mark the beginning and/or end of these stages. The inset shows a close up of the red bump along the red giant branch.

spends on the MS, and it is characterized by the conversion of hydrogen into helium in the core. There are two burning channels through which a star can accomplish this: the proton-proton (pp) chain and the Carbon-Nitrogen-Oxygen (CNO) cycle. In most stars both mechanisms are present but the dominant one is determined by the star's mass and the temperature it can reach in its core. For a $1M_\odot$ star the principal fusion reaction is the pp-chain, but around $1.2M_\odot$ there

is a transition to the CNO cycle which strongly depends on temperature and thus becomes more important for higher masses (Binney & Merrifield, 1998).

Once the star runs out of hydrogen in the core (4) (i.e. reaches the turn off (TO) point) the star becomes a sub giant. We now have an inert helium core and a hydrogen-burning shell surrounding it. In order for the shell to burn hydrogen into helium it must first reach a temperature of $\sim 10^7 K$ (Beccari & Carraro, 2015). Once the shell ignites the hydrogen burning, the density of the regions surrounding the core will decrease, and the core will grow through the addition of helium from the outside shell. In order for the nuclear energy generation to support the whole weight of the star, the core temperature rises slowly which also causes a steady increase of the star's luminosity. To regain equilibrium the star will respond by expanding and cooling the surface while moving towards the region of the CMD dominated by convection (Collins, 1989). At the moment the star is closest to the Hayashi track the sub-giant branch (SGB) ends (5) and the star is now going up the red giant branch (RGB). The time a star spends on the RGB is very mass dependant, the higher the mass the shorter the time on the RGB, becoming non-existent for stars with masses over $15M_\odot$ and very long for stars under $2.2M_\odot$ (Beccari & Carraro, 2015). An important feature of the RGB for low-mass stars, is the red-giant bump, visible on the CMD by the accumulation of stars at a certain magnitude. The accumulation of stars happens as the stars spend more time in this stage of their evolution than in any other part of the RGB. Looking at the the inset on Figure 1.1, we can see the star's evolutionary path going back and forth in luminosity (represented on the CMD as magnitude), these changes in luminosity are believe to be caused by a *"jump in mean molecular weight at the dredge-up composition discontinuity, as a consequence of its effect on the hydrostatic structure of the region immediately above the hydrogen burning shell"* (Christensen-Dalsgaard, 2015) which leads to a small decrease in luminosity. Once the shell leaves the discontinuity the star goes back to moving up the RGB.

The end of the star on the RGB is marked by the helium flash at the tip of the RGB (6), the core of the star is now hot enough to burn helium into carbon, and will still have the hydrogen burning shell around it. The flashes will continue until the temperature of the core is high enough to completely remove the degeneracy of the core and the equation of state reverts to the ideal-gas law (Collins, 1989). The star finally settles at the zero age horizontal branch (HB) where it will continue fusing helium into carbon and oxygen.

When the He runs out in the core (7) the star will start going up the asymptotic giant branch (AGB). Here the star has an inert carbon-oxygen core with a helium burning shell around it and a hydrogen burning shell around that. Once again the envelope expands, the temperature decreases and the luminosity increases. The star starts losing these shells (8) and it becomes a planetary nebula. Temperature increases very quickly (with almost a constant luminosity) until all the gas is dispersed (9). Finally the star starts cooling off and is now a white dwarf (WD).

During the cooling stage there is no nuclear generation of energy and all the energy emitted comes from the stored thermal energy of the WD.

1.1.2 Implications for Globular Clusters

As we mention earlier, stars with higher masses evolve more quickly than those of lower masses, adding the fact that the stars in a cluster are born at the same time[1], this would lead us to expect that any star more massive than the TO should have already evolved off the MS. Figure 1.2 shows two CMDs of 47 Tuc, constructed with data from the Hubble Space Telescope (HST) using, for the left plot, filters in the visible range of the spectrum (F606W and F814W), and the other one using ultraviolet (UV) filters (F225W and F336W, chapter 2 will discuss more about the filters and how the CMDs were obtained). In both CMDs we have highlighted the different branches discussed previously in order to show where each population is, how the shape of the CMD changes with different filters and how different filters favour different stars (the brightest stars on one CMD are not necessarily bright on the other). Tracing the evolution of stars on the CMDs seems like an easy task if we stick to the bulk of the population, however we see the presence of stars above the TO as an extension of the MS. These stars are the BSS, and though they do not make up even 1% of the observed sample they are unexpected, and therefore interesting, members of the cluster.

1.2 Dynamical Evolution of Globular Clusters

To describe the dynamical properties and morphology of GCs relevant to this investigation, only a few main parameters are needed. We mention at the beginning that the observations to complete this research were performed on the core of 47 Tuc. The core radius, r_c, is defined as the radius where the surface brightness distribution drops by half from its central value. There is also the half-light radius, r_h, which contains half the total luminosity of the cluster. For 47 Tuc these values are 21.6 and 190 arcseconds respectively (Harris, 1996).

The dynamics of GCs (or essentially any stellar system) can be described using three different time scales: the crossing time, t_{cross}, the relaxation time, t_{relax}, and the dynamical evolution time, t_{evol}. This last time scale is define by Meylan (2000) as *"the time during which energy-changing mechanisms operate, stars escape, while the size and profile of the system change"*. The crossing time, defined as $t_{cross} = R/\upsilon$ (Binney & Tremaine, 2008) (where R is the radius of the system, and υ, the typical speed of a star), is the time a star takes to cross the system and

[1]There is photometric (Milone et al., 2012a) and dynamical (Richer et al., 2013) evidence that clusters may have indeed two or three different generations of stars. But these would have only occurred within a period of 1 to 2 Gyr (Ventura et al., 2009), not enough to have stars as massive as the BSS.

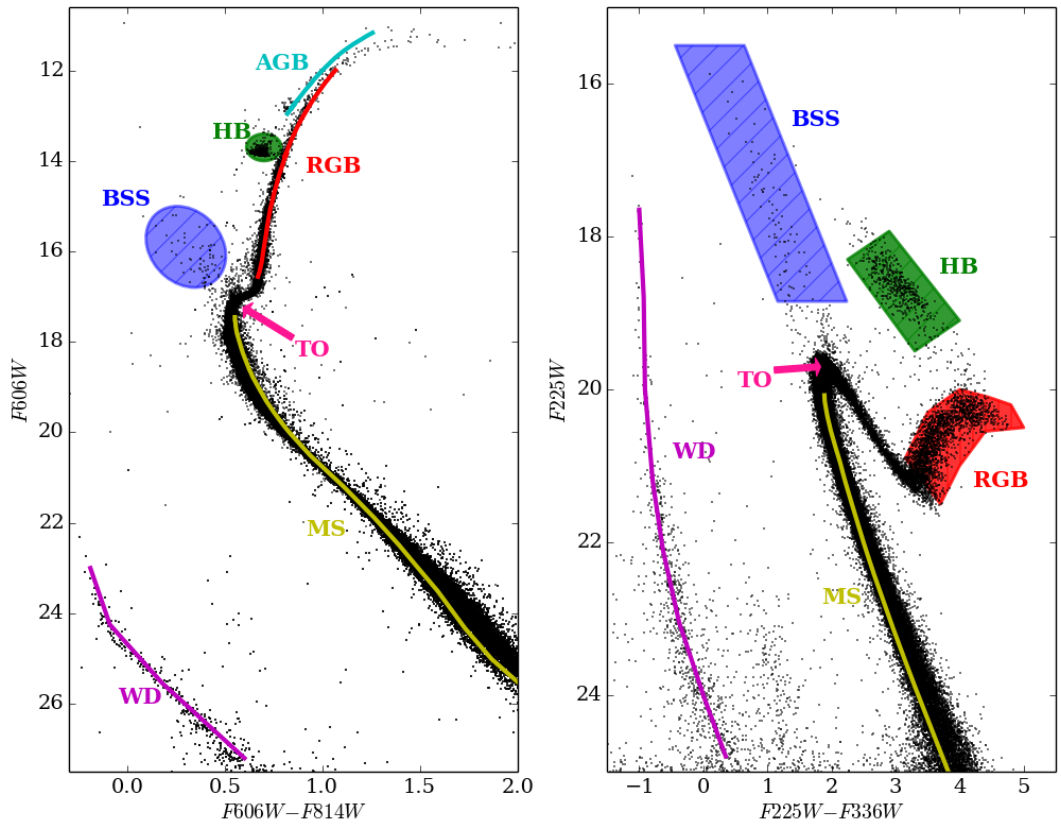

Figure 1.2: Comparing CMDs in the visible (*left*) and UV (*right*) range. The figure shows the differences between the CMDs constructed with the same two sets of filters that we will use for the analysis. To get the same branches on both CMDs, the $F606W, F606W - F814W$ diagram was completed using data from outside the core (HST cycle 17 GO-11677, PI: Richer) as in those filters its not possible to get to such faint stars in the core as the lower MS and WD stars.

its related to the second time scale by:

$$t_{relax} \approx \frac{0.1N}{ln(N)} t_{cross} \tag{1.1}$$

(Binney & Tremaine, 2008) where N is the number of total of stars in the system. The relaxation time is described as the time it takes the system to have its velocity distribution approach a Maxwellian distribution (Spitzer, 1987). For 47 Tuc, the relaxation time in the core is believed to be about 70 Myr (Harris, 1996; Heyl et al., 2015b).

An important process in GC dynamics is mass segregation that happens on a time scale of t_{relax}. Essentially mass segregation means that more massive stars move towards the center of the cluster while less massive ones tend to go towards larger radii, completely changing the

mass distribution the cluster began with. This process is the result of two different mechanisms: relaxation and equipartition. The first one comes from the fact that each star wanders away from its initial orbit increasing the entropy of the system leading it to a new configuration with a small, dense core and and a large, low-density halo (Binney & Tremaine, 2008). The second one comes from kinetic theory which tells us that particle encounters will make those particles with large kinetic energy lose energy to those with lower energies, leading to a state where the mean-square velocity is inversely proportional to mass. In the case of stars, massive ones that lose energy to less massive stars fall towards the center increasing their velocities and gaining kinetic energy but lose it by falling and continue to fall, while less massive stars rise towards the outer parts of the cluster as they slow down (Meylan, 2000; Binney & Tremaine, 2008).

One of the first detailed studies of mass segregation fin 47 Tuc was carried out by Anderson (1997). Using images of the core of 47 Tuc, he was able to measure the luminosity function to which he fitted King-Michie models obtaining the best agreement with those models that included mass segregation. But not only can mass segregation be analysed through luminosity functions, if the core of a cluster is indeed relaxed, the radial distribution of different groups of stars should also exhibit indications of this phenomenon and 47 Tuc should not be the exception. We will show in Chapter 4 how the high quality of this data set, allows us to display evidence of mass segregation in the core of 47 Tuc by using the mass difference between MS stars of different magnitudes (or mass). This process will also lead us to an estimate of the masses of the stars in the different sequences visible in our CMD.

1.3 Blue Stragglers

In the last two decades BSS have been found in many GCs as well as open clusters (de Marchi et al., 2006; Ahumada & Lapasset, 2005), in dwarf galaxies (Santana et al., 2012) and in the field of our galaxy (Santucci et al., 2015). Although there is a large amount of observational data revealing important characteristics about BSS, observations alone cannot tell us how or when BSS were formed. Determining the possible formation channels and which ones dominate in the different environments requires models of formation mechanisms and statistical analysis.

In order for these stars to look brighter and bluer than the TO, they had to go through some rejuvenating process as there is no evidence of recent star formation episodes in the environments where BSS live. The BSS formation mechanisms can be divided in many different ways but they all must comply two main conditions: *i)* there must be at least one MS star involved, and *ii)* one of the stars involved must gain mass in order to rejuvenate. In fact, the positions of BSS on the CMD suggest that these stars are in fact more massive than the TO stars. The first attempt to directly measure the mass of a BSS was done by Shara et al. (1997), studying one of the brightest BSS in the core of 47 Tuc, they found a mass of $1.7 \pm 0.4 M_{\odot}$, almost twice

the cluster TO mass of $\sim 0.9M_{\odot}$ (Hesser et al., 1987; Thompson et al., 2010). Later on, different studies, including some done on variable BSS, have yielded masses between $\sim 1-2M_{\odot}$ for BSS in different GCs (Gilliland et al., 1998; De Marco et al., 2005). Recent results for pulsating BSS have provided a lower upper limit of $\sim 1.5M_{\odot}$ (Fiorentino et al., 2014, 2015).

In an attempt to recreate the observed BSS populations and their characteristics many scenarios for the formation of BSS have been proposed, successfully explaining some cases but failing in others. As we have already mentioned what they have in common, the first difference we can make then is through which process the mass exchange happens. Following Figure 1.3, we have two mass gaining mechanisms: mass transfer or merger. How we get to this channels is a much longer story. We will separate the initial scenarios into three different categories following the divisions chosen by Perets (2015): *i)* direct collisions of stars, *ii)* stellar evolution of primordial binaries, and *iii)* dynamical evolution of hierarchical triple systems.

At some point, the line between the formation mechanisms becomes hazy, for example, hierarchical triple systems can form from binary-binary (b-b) interactions (Antonini et al., 2015), at the same time we a can consider b-b interactions as collisions. As in the latest review (Boffin et al., 2015), we will consider any fast dynamical encounter, involving single stars or binary systems, as collisions. Considering this issue, we will summarize the characteristics of the different formation mechanisms and their end products, indicating the points at which the divisions between the formation channels become unclear.

1.3.1 Evolution of Primordial Binaries

Stellar evolution of the individual stars composing a binary system can lead to mass transfer (MT) from one member of the system to the other. This process was first proposed as the possible origin for BSS by McCrea (1964), around ten years after their discovery. He claimed that, having enough MT between the members of a close binary system, the secondary star, to which the mass has been transferred, will end up as an apparently young star. He also predicted this process could lead to BSS of up to 2.5 magnitudes brighter than the TO, not too far away from the values observed today for BSS in stellar clusters.

To predict the outcome of the evolution of a binary system, several characteristics have to be considered. The most important one of these is the stellar evolutionary state of the donor star, which also defines the classification system of cases of MT in binaries introduced by Kippenhahn & Weigert (1967). These cases are divided in:

- **Case A:** MT during MS.
- **Case B:** MT beyond MS but before helium ignition.
- **Case C:** MT beyond helium ignition

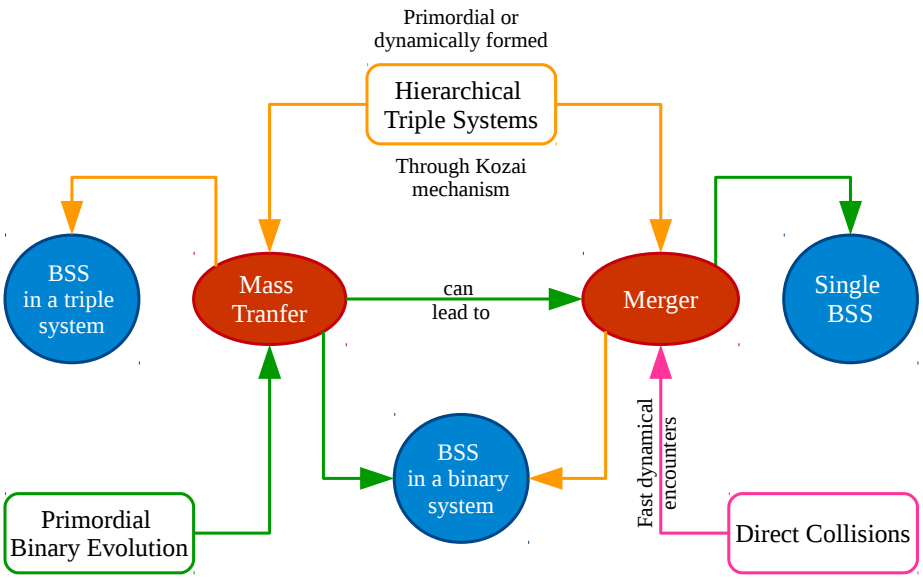

Figure 1.3: Summary of proposed formation mechanisms. The red ovals show the two possible mass gaining mechanisms while the blue circles have the resulting BSS or BSS system. The different coloured rectangles are the three possibles initial scenarios and following the same coloured arrows one can get to the final product of the process. For the direct collisions mechanism the paths to the final products has been left out as, depending on the number of stars involved, they can lead to all the possible end products.

as explained by Perets (2015). Other important aspects to consider are the structure of the donor's envelope, the mass ratio of the binary, and the type of the accretor, which are not only key in determining the end product but are also responsible for the stability of the mass transfer process (Ivanova, 2015).

We will now turn our focus to the conditions that allow a binary system to evolve to form a BSS. Independently of which case of MT the binary follows, the primary star needs to have enough mass available to transfer to the secondary, to make this last one more massive than the TO stars of the cluster (Davies, 2015). Having sufficient mass, the different cases will give BSS with different characteristics, with the mass of the resulting BSS strongly depending on the initial binary orbit (Sills, 2010).

Case A can either form a single massive BSS, if the MT leads to a merger, or a BSS in a short period binary system (Perets, 2015). This is one of the examples where is hard to differentiate from one formation mechanism to the other. For a binary system, consisting of

two MS stars, to have a small enough initial separation to exchange mass, it is believe that a process outside from the natural evolution of the stars needs to take place (Perets & Fabrycky, 2009), for example the perturbation from a third star (Fabrycky & Tremaine, 2007).

In order for case B and C to form a BSS, the binary system contains a post MS star that should not go through a common envelope stage (Hjellming & Taam, 1991) with its companion. The resulting BSS, would end up in higher period binaries compared to case A, with a helium WD companion for case B and a carbon-oxygen WD for case C (Perets, 2015). The mass of the BSS is not expected to be very high for these cases, getting very close to that of the TO especially for case C.

1.3.2 Direct Stellar Collisions

The first to claim a possible collisional origin for BSS was Hills & Day (1976) during a study of stellar collisions in GCs. Their research indicated that a MS star in the dense cores of GCs had a 3% chance of colliding with another MS star during the lifetime of the cluster, chances went up for when one of the stars was in its giant stage. If these these interactions were followed by coalescence, the product would be a BSS.

Following the Hills & Day reasoning, Davies (2015) states two conditions that need to be met in order for a collision to form a BSS: first, the collision must lead to the merger of the involved stars, and second, the end product of the collision must look more massive than the TO stars of the cluster (a rejuvenated star with a mass below that of the TO of a system will not be observable as a BSS on a CMD). In fact, for low velocity encounters, collisions are believed to be very effective conserving most of the mass of both merged stars (Benz & Hills, 1987).

Even though the stars are rejuvenated, they are not reborn, as pointed out by Sills (2010), BSS resulting from collisions are thought to evolve in a similar manner as normal stars of the same mass, however they are expected to have shorter MS lifetimes. The reason behind this assumption comes from the fact that the new star is made up of stars that had already been evolving for some time and thus the initial amount of hydrogen in the core is smaller compared to a zero age MS star of the same mass. According to Lombardi et al. (1996), for stars of nearly equal mass, the collision product does not fully mix, instead, the cores of the participating stars end up as the core of the new BSS. In this case, if both stars are close to the TO mass, the BSS will not have a very long MS lifetime. In contrast, in collisions involving stars with a mass ratio ≤ 0.5, the hydrogen rich smaller star settles in the core of the merged product, adding not only the remaining hydrogen in its core but also the hydrogen shell around it, producing a longer MS lifetime compared to the equal mass case.

Direct collision of stars do not only happen between single stars (s-s), but binaries can also be involved. Single-binary (s-b) and b-b encounters are also possible and more likely than s-s collisions (Sills, 2010). Encounters involving binary systems will be significant when another

star or binary passes within a distance equivalent to the size of the binary (Davies, 2015). The product of these collisions between more than two single stars can leave behind more massive BSS exceeding twice the TO mass (Fregeau et al., 2004), with a long period ($\gtrsim 10^3$ days) binary companion (Chatterjee et al., 2013).

1.3.3 Dynamical Evolution of Hierarchical Triple Systems

The last option for the origin of BSS is much newer compared to the previous ones. Iben & Tutukov (1999) were the first to describe an scenario where a hierarchical triple system (a third star is orbiting the inner binary) would actually evolve to become a BSS in a binary system. A few years before Leonard (1993) had a similar idea, but he discarded this possibility claiming there would need to be a much higher triple system frequency than the one observed at that time and went back to the physical collisions theory.

With the discovery of triple systems harbouring BSS (see van den Berg et al. (2001) for an example), and the disagreement between the observed BSS populations and that obtained from combined N-body and stellar evolution simulations that considered only collisions and primordial binary evolution, the study of BSS formation through triple systems evolution became an independent subject of study. Perets & Fabrycky (2009) claimed that previous BSS formation studies demanded a fraction of the primordial binaries to be short period binaries which a previous publication by one of the authors (Fabrycky & Tremaine, 2007) had shown that such systems actually come from longer period binaries that have been perturbed by a third star via the Lidov-Kozai mechanism (Lidov, 1962; Kozai, 1962). In fact, studies done on short period (Tokovinin, 1997) and contact (Pribulla & Rucinski, 2006) binaries showed that at least 40% of these systems have distant companions.

Recent studies following the formation channel proposed by Perets & Fabrycky, indicate that the Lidov-Kozai mechanism has a 21% efficiency when it comes to forming tight binaries (Naoz & Fabrycky, 2014). And, when applied to GC systems, it can contribute up to 10% of the total BSS population (Antonini et al., 2015). This population should show some observational differences when comparing them to the BSS from the binary mass transfer scenario. For instance their mass could reach much higher values than cases B and C, where part of the mass of the system is left in the WD companion. The WD is also another difference as BSS from a triple system are more likely to be left with a MS companion (Perets, 2015).

1.3.4 Linking Models to Observations

All the above formation mechanisms are able to reproduce the observed properties of single BSS. But when we observe a system of stars such as a stellar cluster, we are analysing a population and not single stars. For a formation mechanism to produce an compelling number of BSS such that it yields a notable observable population, it must occur at a significant rate,

and the end products must have a lifetime long enough to accumulate (Davies, 2015). Which mechanism dominates in the different environments where BSS live is still in debate. Although not definite answer has been reach most studies agree that the observed populations today are a result of a combination of all the formation channels, with one mechanism prevailing over the others depending on the system's properties.

When trying to reproduce the observed populations of BSS in clusters including all the factors becomes an almost impossible task. Besides having simulations producing BSS through the different mechanisms, the dynamical evolution of the cluster also needs to be taken into account. One important effect of dynamical interactions is that, over time, these will alter the binary population of a system. Heggie (1975) showed that dynamical encounters in N-body systems will make tight binaries tighter while soft binaries are likely to be destroyed. This statement is supported by the anticorrelation found by Milone et al. (2012b), between binary fraction and absolute luminosity (mass).

Attempts to find the dominating formation mechanism in different GCs, have been based on finding the strongest correlation between the number of BSS and parameters of the cluster, like total or core mass, binary fraction and collision rate, that are some how related to the different formation channels. Early studies that compared models to observations found no important correlations, for example (Piotto et al., 2004), noticed no correlation between the number of BSS and any of the cluster parameters except for a very low dependence on the central density. As it was very difficult to get good photometric data in the dense cores of GC, it wasnt until 2009 when Knigge et al. found a strong correlation between the number of BSS in the core and the core mass, concluding that most of the BSS come from binary systems, but at the same time these binaries could have been affected by dynamical encounters. With the results pointing towards a binary origin for BSS, researchers started to look for confirmation of the correlation between BSS frequency and binary fraction already found by Sollima et al. (2008) in low density GCs. Milone et al. (2012b) reaffirmed this correlation for a sample of 59 GCs. Leigh et al. (2013) also tried to find a relation between binaries and BSS but their results showed a much stronger correlation with the core mass as found by Knigge et al. (2009), despite the fact that binary fraction in GCs anticorrelates with core mass (Milone et al., 2008). One of the latest studies that included dynamical effects and stellar and binary evolution yielded *"a dependence of blue straggler number on cluster mass, a tighter correlation with core mass, a weak dependence on the collisional parameter, and a strong dependence on the number of binary stars"* (Sills et al., 2013).

To compare the observed BSS to the modelled BSS population, many studies use the radial distribution of these stars, not only to compare them to models but also to other populations in the same system. The analysis of the observed radial distributions all agree that, for stellar clusters, the BSS are more centrally concentrated that the rest of the populations (Perets, 2015)

which according to mass segregation means that they are more massive than the average star. Other interesting results have been the discovery of bimodal distributions for BSS in GCs like M3 (Ferraro et al., 1997), 47 Tuc (Ferraro et al., 2004), M55 (Lanzoni et al., 2007) and NGC 6229 (Sanna et al., 2012). These distributions, in general, show a peak in the cluster center, decreasing at intermediate distances from the center, to rise again in the outskirts. A good explanation for this bimodality, was presented by Mapelli et al. (2006) where they conclude that the BSS in the external regions are almost entirely product of mass transfer in primordial binaries, in contrast, core BSS are more likely to have originated from collisions. Additional observational evidence in favour of the mixed formation mechanism, is the two distinct sequences of BSS observed in the GC M30 (Ferraro et al., 2009). Here the authors claim that the bluer BSS have a collision origin while the redder BSS are the product of the evolution of close binaries.

1.3.5 Blue Stragglers and 47 Tucanae

In the particular case of 47 Tuc, the study of its population of BSS started with the discovery of 21 of such stars in one of the first HST observations of the core of this cluster (Paresce et al., 1991). This small sample of BSS already showed signs that the density of BSS is higher in the central regions of the cluster. Many investigations on the topic have taken place since then, before the discovery of the mentioned bimodal distribution in 47 Tuc, Sills et al. (2000) modelled the formation rate of BSS using data outside the core. The results obtained by the authors suggested that 47 Tuc may have stopped making BSS several billion years ago, undergoing an epoch of enhanced BSS formation around the same time possibly connected to the epoch of primordial binary burning.

Following the discovery of the bimodal distribution, different attempts to explain the spatial layout of BSS in 47 Tuc were made. Mapelli et al. (2004) tried to reproduce the BSS radial distribution by choosing different formation mechanisms: collisional BSS in the innermost region and primordial binary evolution outside the core. The best representation of the observational data was obtained when 25% of the BSS come from binaries and 75% from collisions within $0.5r_c$. This result was later refined by Mapelli et al. (2006) obtaining a best fit when 46% of the BSS come from mass transfer and 54% from collisions. The models were also able to predict the minimum in the radial distribution and its surrounding regions named by Mapelli et al. (2004) the *"zone of avoidance"*, with the condition that external MT BSS production began beyond $30r_c$.

Later on, Monkman et al. (2006), tried to explain the bimodal distribution with a purely collisional model throughout the cluster. Their results agreed with those found by Mapelli et al. (2004, 2006) for the core of the cluster where the collisional model represents the observational data. For their middle region (between 23 and 130 arcseconds) BSS formation would have

needed to stop about half a billion years ago. But for the external regions the collisional models were not able to predict the BSS population, a result that they concluded is likely due to another formation mechanism dominating the outskirts of 47 Tuc.

Around the same time the formation mechanisms debate was taking place, researchers found evidence that BSS in the core of 47 Tuc have masses larger than twice the MS TO mass. One result that suggested the presence of massive BSS was found by McLaughlin et al. (2006), while studying the proper motion and dynamics of the cluster core, determined that the velocity dispersion of BSS was smaller than that of the cluster giants by a factor of $\sqrt{2}$ (i.e. twice their mass). That same year, Knigge et al. (2006) identified a detached binary system consisting of a $1.5M_{\odot}$ BSS primary with an active, upper MS companion. These massive BSS can only be the outcome of a process involving at least three progenitors.

Another interesting area of research is the evolution of BSS. One piece of observational evidence that suggests where evolved BSS might live on the CMD is presented by Beccari et al. (2006). The authors examined the bright end of the CMD and found an overabundance of massive stars in the AGB of 47 Tuc and concluded that they could be possible related to the evolution of binary systems. This presence of extra stars had already been noticed by Bailyn in 1994, who also linked them to the evolution of BSS. We will carry a more detailed analysis of this topic in section 6.2.

Chapter 2

Observations and Data Analysis

Although obtaining photometry of GCs seems like a direct process, it comes with some complications, most of them due to the high stellar density of these systems, especially in or near to the core. Stars are so close together that, even with the best observing conditions and technology, it is very likely to miss some of them, particularly towards fainter magnitudes. To avoid any misinterpretation of the data caused by missing sources, we resort to point-spread-function (PSF) photometry (section 2.1) to optimize our object detections, and artificial star tests (section 2.2), for incompleteness corrections.

2.1 Observations and Photometry

The data come from observations made with the Hubble Space Telescope (HST) using Wide Field Camera 3 (WFC3) with two of the most ultraviolet (UV) filters, F225W and F336W, whose central wavelengths are 235.9 nm and 335.9 nm respectively. Ten fields in the core of 47 Tuc were obtained between November 2012 and August 2013 during cycle 20 of the HST program GO-12971 (PI: H. Richer). The observations were planned so that each visit included two exposures in each filter, 380s and 700s for F225W and 485s and 720s for F336W. Each field was offset from the previous one to map the entire central region of the cluster as shown in Figure 2.1. The combined field of view covers a radius of ~ 160 arcseconds from the center of the cluster.

The data analysis was performed following the procedure described in Kalirai et al. (2012). First the observations were retrieved from MAST (Barbara A. Mikulski Archive for Space Telescopes). All the images were then corrected for geometric distortions using MultiDrizzle (Fruchter & Sosey, 2009). The next step was to register the images onto the same reference frame, using DAOPHOT II (Stetson, 1987) we selected the brightest stars in each image and obtained their positions to calculate the transformations between each field and the reference. The transformations were then put together in a shift file which MultiDrizzle uses to make one

drizzled image for each filter. Finally, using DAOPHOT II and ALLSTAR (Stetson, 1994) PSF photometry[1] was performed in both the stacked images, and the magnitudes were zero pointed to the VEGAMAG (Bohlin & Gilliland, 2004) photometric system[2]. The two final photometry files are matched into a single catalogue resulting in the UV CMD depicted, for example, in the figure in the left panel of Figure 2.3. It is important to mention that as we will be analysing radial distributions, the star like shape of the final field has been reduced to a circular area centred in the center of 47 Tuc as shown by the blue circle on Figure 2.1.

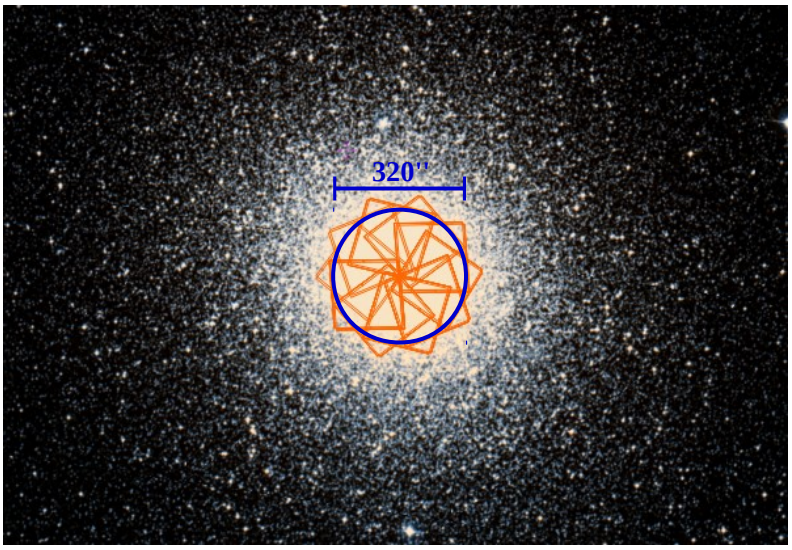

Figure 2.1: GC 47 Tucanae and the observed field. This image was generated using the AstroView Tool of MAST Data Discovery Portal. The background image is part of the Digitized Sky Survey and was taken by the UK Schmidt Telescope at Siding Spring Observatory in New South Wales, Australia. The orange squares represent the WFC3 fields. The blue circle and dimension indicator are superposed to show the actual field used for this research and its diameter.

2.2 Artificial Star Tests: Correcting for Incompleteness

To estimate the number of stars lost in the photometry process, we ran artificial star tests. The procedure, explained in detail in Heyl et al. (2015b), consists in inserting artificial stars into the

[1]DAOPHOT runs aperture photometry on all the stars above a threshold, from which it picks a set of well defined stars to build a PSF. Finally it measures the positions and magnitudes of all the stars that match the PSF in the field.

[2]The magnitudes observed are instrumental magnitudes, VEGAMAG is a system to convert these magnitudes into a common photometric system. VEGAMAG gets its name from the star Vega (a bright AOV star in the constellation Lyra with a very smooth spectrum), and is defined such that the magnitude of Vega is 0 at all wavelengths.

images in both F225W and F336W filters and calculating how effectively these are recovered when run through the same photometry process as the real stars. The completeness rate is a function of both the magnitude of the star and its distance from the center of the cluster, and so, artificial stars were given a range of values covering the observed magnitudes and distances to the center of 47 Tuc. As can be seen in Figure 2.2, the completeness rate is strongly dependent on both radius and magnitude, with only the brightest stars close to unity.

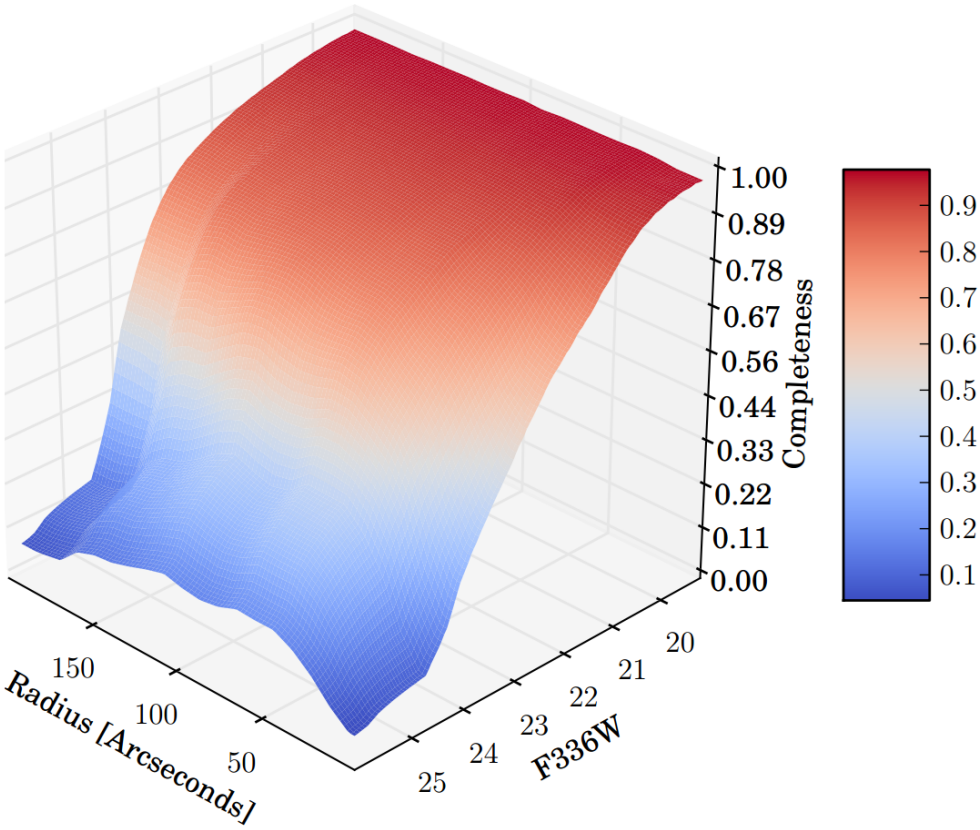

Figure 2.2: Completeness rate as a function of the distance from the center of the cluster and the magnitude of the artificial star.

To test our correction for incompleteness, we compared the radial distribution of the Small Magellanic Cloud (SMC) to that of R^2. The SMC is a dwarf galaxy orbiting the Milky Way which happens to lie in the background of 47 Tuc. The two objects are completely unrelated and very far apart (47 Tuc is 4.5 kpc Harris, 1996, away from the Sun, while the SMC is at $\sim$ 60 kpc, Hilditch et al., 2005), but since they share the same sky area, stars from the SMC contaminate the CMD of 47 Tuc. Figure 2.3 shows where the MS of the SMC lies on our CMD. Because the SMC is not related to 47 Tuc, the radial distribution of its stars should be proportional to the area of the field of our observations. Looking at the right panel of

Figure 2.3, we can see the comparison between the incompleteness corrected cumulative radial distributions of the SMC and R^2 (as we are only counting the stars within a circular area). If our completeness rates were properly obtained then these distributions should be approximately equal. In fact the KS-test yields a p-value of 0.60 telling that we cannot reject the hypothesis that the distributions are in fact the same. The mean completeness fraction of the SMC sample is less than 70%, so the completeness correction is crucial to obtaining the estimate of the underlying distribution.

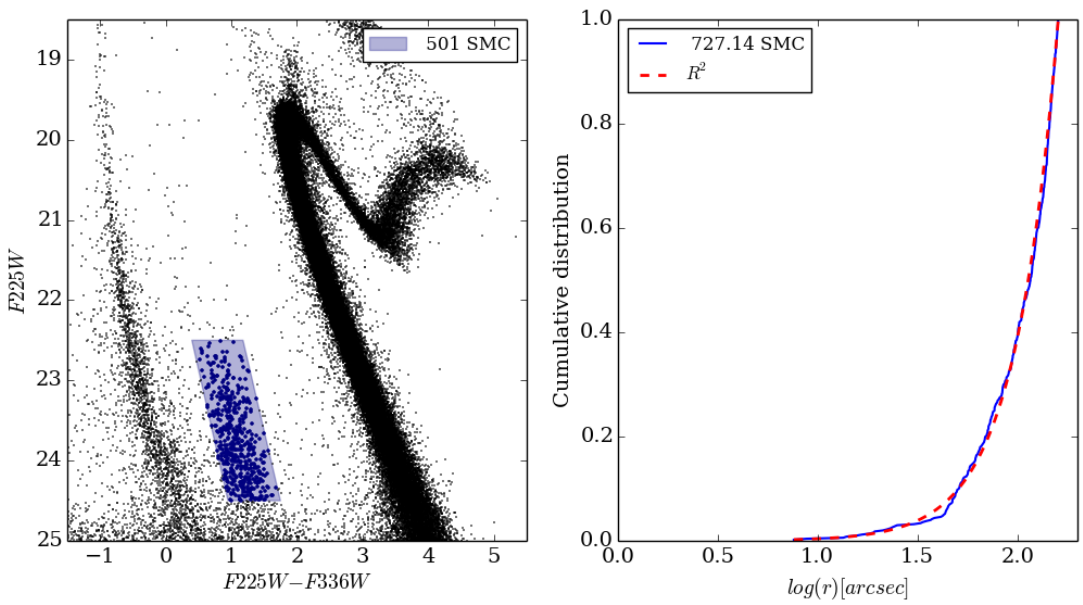

Figure 2.3: *Left:* Selection of SMC stars on the UV CMD. *Right:* Cumulative radial distribution of the SMC compared to R^2. The legend on the CMD indicates the number of stars before correcting for incompleteness, while the legend in the right plot gives the size of the sample after correcting for incompleteness. The agreement between both distributions allow us check the validity of our completeness rates.

2.3 The ACS Data Set

The data used to construct the CMD in the visible range (hereafter the ACS data) was obtained from the ACS (Advanced Camera for Surveys) Survey of Galactic Globular Cluster Sarajedini et al. (2007). The survey used the ACS Wide Field Channel to obtain photometric data of 65 of the nearest globular clusters and is publicly available at: http://www.astro.ufl.edu/~ata/public_hstgc/databases.html. A description of the data reduction and photometry can be found in Anderson et al. (2008).

Chapter 3

Stellar Population Selection

Due to the high quality of the data, each population is easily identified and can be separated one from another. Each population is defined to be within a region shown by the different color boxes in figures 2.3 through 5.3. The boundaries of each region were chosen with the help of MESA evolutionary models, slight modifications on the limits of these regions would only make including stars with higher photometry errors or not real members of the different branches more likely. Also, including the stars surrounding the highlighted regions does not change the number of stars in each box by more than a few percent and tests done including these stars show no effect on the shapes of the cumulative radial distributions.

3.1 Main Sequence Binaries

In an attempt to identify the population of stars responsible for the formation of BSS, we will later compare the BSS distribution against the binary stars distribution. We have selected a sample of main sequence binaries (MSBn) that we expect to be mostly nearly equal mass binaries. Both populations are shown on Figure 3.1. The MSBn selection box starts at a magnitude value of 24 and extends up to brighter stars by about 3 magnitudes with an almost constant width of 0.4 magnitudes (width reduces at the brighter end of this selection box to avoid contamination by SGB stars) containing a total of 367 stars number that goes up to $\sim$438 after correcting for incompleteness.

We have also included a selection of stars on the main sequence (MS) to have a reference for the analysis of this population. To ensure there is no contamination to the MSBn samples, a minimun distance of ~ 0.2 magnitudes is kept between the binary sequences and its single star sequence counterpart.

Looking at the right panel of Figure 3.1, we can see that the cumulative radial distribution for the MSBn is much more centrally concentrated than that of the single MS stars.

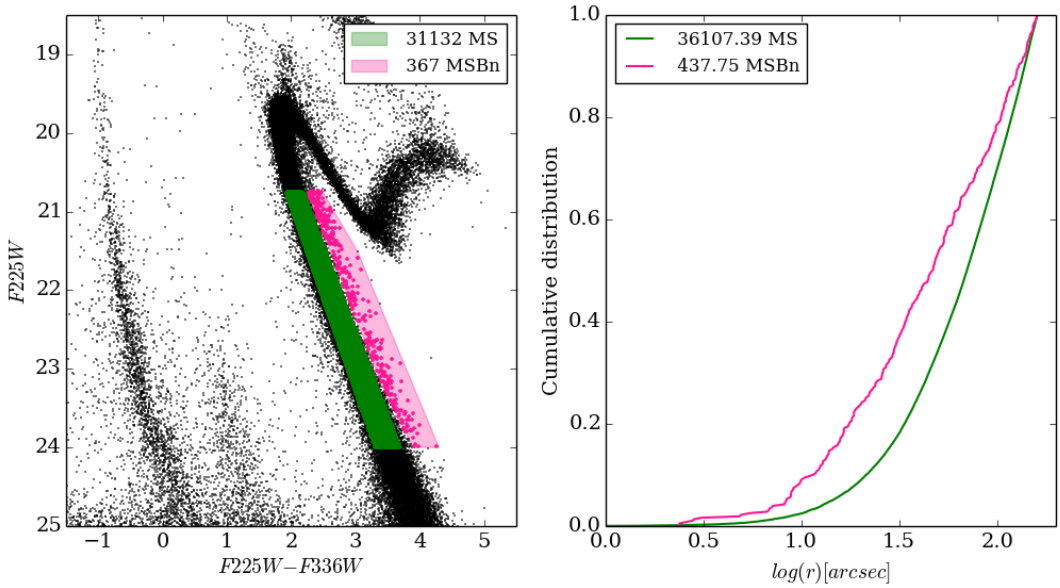

Figure 3.1: *Left:* $F225W, F225W - F336W$ CMD showing the selected stars for the MS and MSBn. *Right:* Radial distributions for the selected samples. The inset on the CMD has the number of stars before correcting for incompleteness, while the one in the right panel gives the size of the sample after correcting for incompleteness.

3.2 Blue Stragglers

As can be seen in Figure 3.2 the BSS population is easily spotted on the UV CMD as an extension of the MS of the cluster. Starting a few tenths of magnitudes above the turn-off point and extending for almost 4 magnitudes, the total number of BSS on the sample goes up to almost 150 stars. For this study, we have decided to exclude the very faint BSS, and taken only those that are at least ~ 0.7 magnitudes brighter than the TO, to avoid any possible contamination due to blends. This decision was also based on the fact that when we plot the BSS sample on the ACS CMD, the fainter BSS on the UV sample are very close to the $F606W, F606W - F818W$ TO, almost blending with the MS and it is important that we have clean BSS samples on both CMDs.

After delimiting the BSS sample we end up with 114 BSS, which we divide into two subsamples, faint and bright BSS. Each smaller sample started with half the stars of the original, with the bright BSS (bBSS) distribution looking much tighter than the faint BSS (fBSS). In order to obtain two distinct BSS populations we have maximized the difference between their radial distributions ending up with 58 bBSS and 56 fBSS, with the bBSS extending across a much larger range in magnitude (2.5 magnitudes) compared to the faint sample (0.85 magnitude). Figure 3.2 shows the final divided BSS samples and their corresponding radial distributions compare to the reference population explained in the next section.

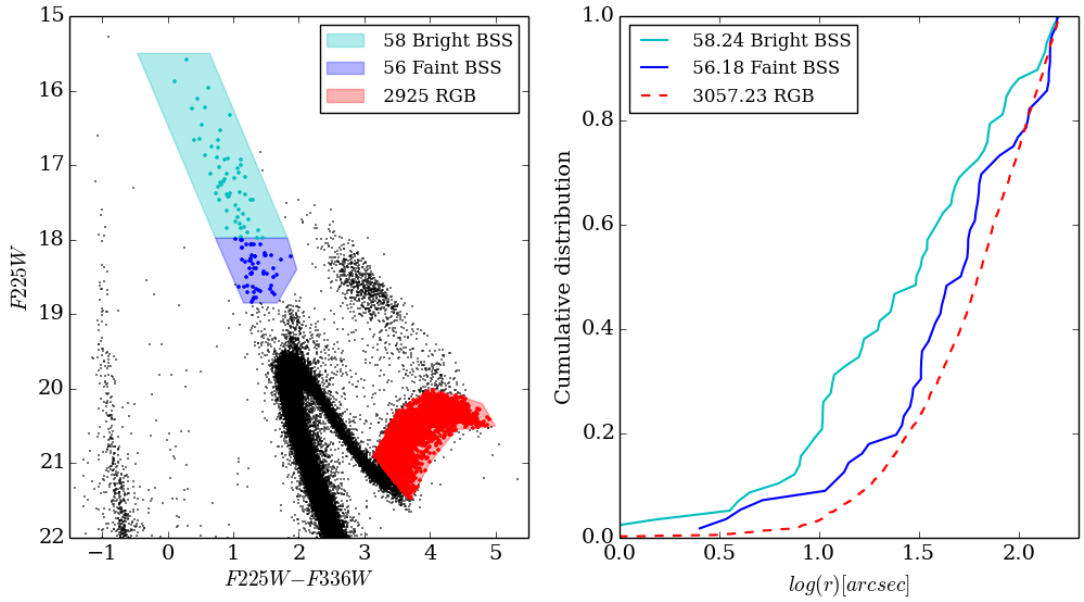

Figure 3.2: *Left:* $F225W, F225W - F336W$ CMD showing the selected stars for the faint and bright BSS and RGB. *Right:* Radial distributions for the selected samples. The legend on the CMD has the number of stars before correcting for incompleteness, while the legend on the right plot gives the size of the sample after correcting for incompleteness. The division between bright and faint BSS was chosen by maximizing the difference between their radial distributions in order to obtain two distinct BSS populations.

3.3 Reference Population

To trace the cluster stars we selected the RGB as the reference population. Although previous studies (Ferraro et al., 2003, 2004) indicate the HB as the most natural reference population, in the UV CMDs, due to this branch being well separated from other branches, we are concerned with the contamination of the HB by AGB stars and evolving BSS which will be discussed later on chapters 5 and 6.

In the UV, specifically with the filters chosen for this work, the RGB is well defined and easy to identify on the CMD. Even though the RGB is not separated from the SGB the shape of the CMD makes it easy to get a clean sample. To make sure there is no contamination of SGB stars on our RGB sample, we start our RGB box a few tenths of a magnitudes above and to the right of the end of the SGB. The box pointed out in red on Figure 3.2 shows the final selection for the reference population with a total of 2925 stars before completeness correction and a smooth radial distribution corrected for incompleteness coming to a total of $\sim$ 3050 stars.

As mentioned in previous chapters, we will compare our data to the ACS sample. On the ACS CMD, the RGB, especially in the fainter part of this branch, is also well defined. Cross

matching the selection of the RGB on the UV CMD to the visible range CMD, also gets us a clean RGB sample of stars starting around ~ 0.5 magnitudes brighter than the TO, which tells us that our efforts to exclude SGB stars from our UV sample were successful. Even at the bright end of the RGB on the visible range CMD we can see that this branch is well separated from the horizontal and asymptotic giant branches, making it a suitable reference population also in these filters. Because the ACS field is smaller than the WFC3 field, we also expect our RGB sample to be smaller, coming to a total of ~ 2200 stars compared to the ~ 3000 we had before.

3.4 ACS Data Selection

In previous sections we mention the concern about the contamination of the HB by AGB and evolving BSS stars. In an attempt to try to identify the stars polluting the HB we select what we think is a cleaner sample of HB stars in the ACS CMD which we call faint HB. In order to be able to compare the ACS and WFC3 data sets, the data for $F225W$ and $F336W$ were reduced to the same field as the the one covered by the $F606W$ and $F814W$ which is also in the core but expands to a radius of only 105 arcseconds. In order for a star to be used in this research, it had to be measured in all four filters.

As in the WFC3 CMD we used MESA models to choose our regions which are shown in Figure 3.3. The detailed reasoning behind the division of faint and bright HB stars and the difference between the AGB and the bump on this branch will be explained in chapters 5 and 6. The important point for now is confirming the presence of non-HB stars on the HB of the UV CMD that can be pictured on the right panel of the figure. Using the same color code as on the left panel we can see how bright HB, AGB and the stars on the bump of the AGB picked on the ACS CMD, fall on the same region as the HB stars on the WFC3 CMD. Although we lose some stars as we had to reduce our field to match the ACS field, we can identify where the AGB from the evolution of normal stars fall in the UV CMD and obtain a cleaner sample of HB stars, leading to the proper classification of over 100 stars that we would have otherwise needed to ignore.

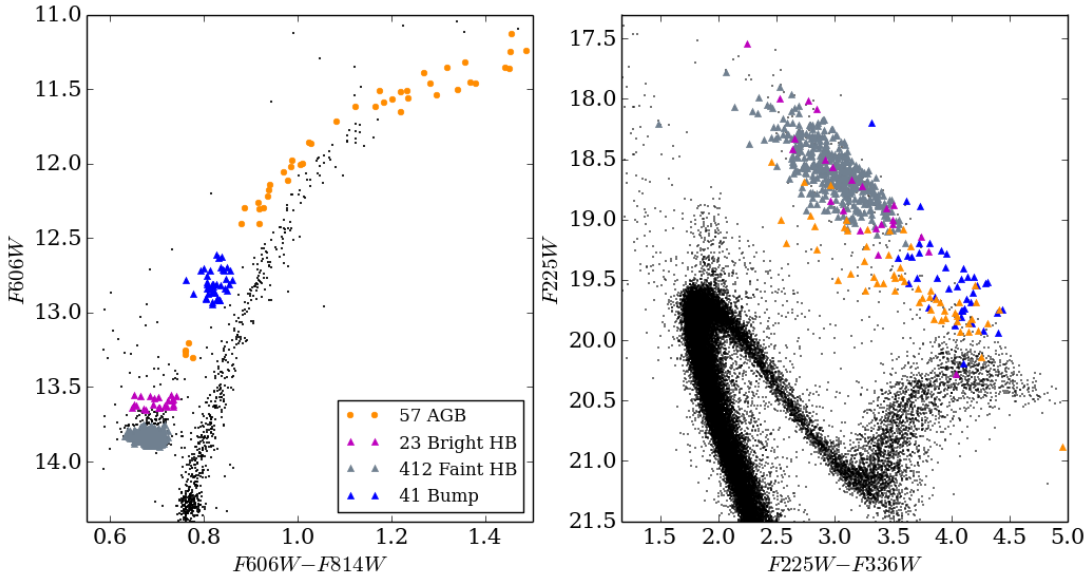

Figure 3.3: *Left:* $F606W, F606W - F814W$ CMD with the selection of the stellar populations on the ACS data. *Right:* $F225W, F225W - F336W$ CMD showing where the stars selected on the ACS data fall on the UV CMD. We can see a clear contamination to the UV HB by stars on stellar evolutionary stages different from the normal HB but that form clear branches on the ACS CMD. The number of stars for each sample is given in the inset in the left plot.

Chapter 4

Estimating Masses Outside the MS

Although our main focus is not mass segregation, the analysis of the BSS population in the core of 47 Tuc requires that we have knowledge about the masses of the stars along the many evolutionary stages and whether or not they have relaxed. As we mentioned in section 1.2, the high quality data and photometry have allowed us to go as faint as 6 magnitudes below the TO reaching a significant enough mass difference along the MS to be able to show mass segregation. Figure 4.1 shows the CMD of 47 Tuc in the UV, where we have highlighted three MS regions with the corresponding masses at the center of each box based on an 11 Gyr PARSEC isochrone (Bressan et al., 2012)[1] constructed using the metallicity of 47 Tuc and the bolometric corrections of Chen et al. (2014). In order to fit the isochrone to the data, besides the distance modulus ($(m-M)_0 = 13.36$, Woodley et al. 2012) and reddening ($E(B-V) = 0.04$, Salaris et al. 2007) it was necessary to add 0.4 and 0.3 magnitudes of extinction to F225W and F336W respectively. The isochrone fits the CMD in F606W and F814W without any additional corrections. To the right of the CMD we have the radial distributions of the different MS regions, we can see how the brightest and more massive MS stars are significantly more centrally concentrated than the faintest sample, with the intermediate mass sample sitting in between. The observable difference between the distributions can be confirmed with a KS-test which yields p-values of the order of 10^{-21} or lower.

We can now use the radial distributions to predict the masses for different groups of stars in 47 Tuc. For each of the three MS regions we take the value of the distance from the center of the cluster where the cumulative distributions reach 20 and 50 percent, we call these distances R20 and R50 respectively. Plotting the logarithmic values of each mass against their corresponding R20 and R50, we find a relationship for each R. The logarithmic values of mass (M) and R

[1] Available at http://stev.oapd.inaf.it/cmd

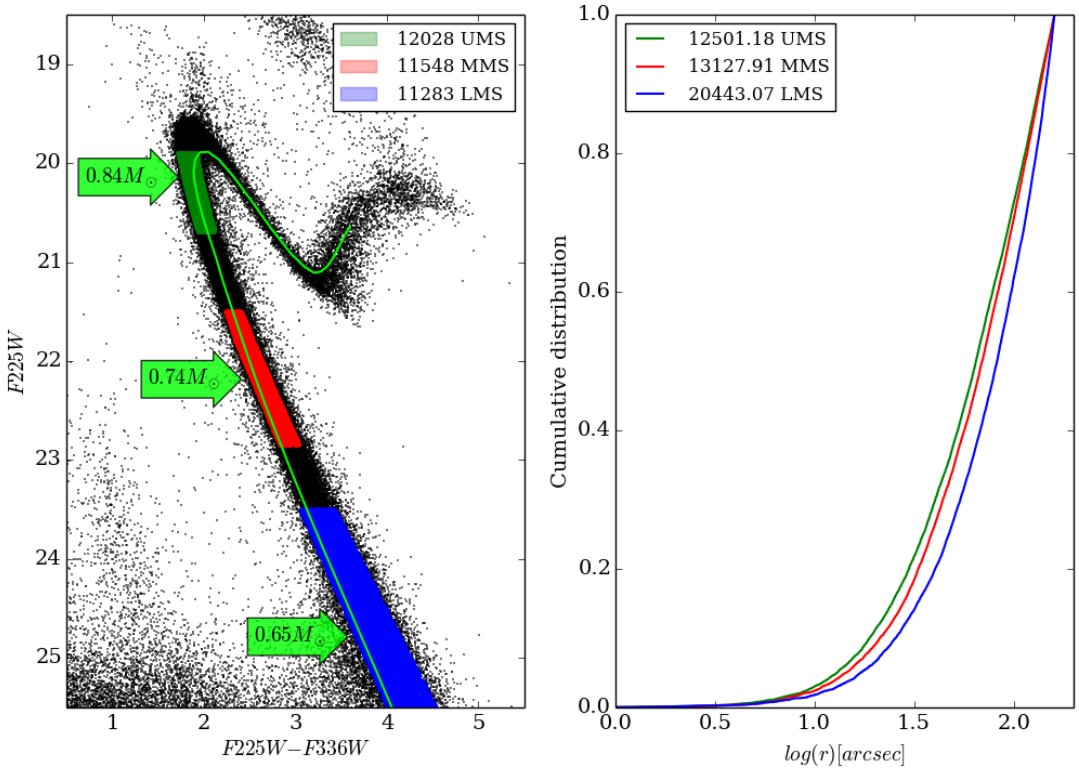

Figure 4.1: *Left:* UV CMD of the core of 47 Tuc displaying the selection of three MS regions, upper, middle and lower MS, with the green arrow boxes showing the corresponding masses at the center of each box based on an 11 Gyr PARSEC isochrone. *Right:* Radial distribution of the regions pointed out on the CMD following the same colour pattern. The legend on the CMD has the number of stars before correcting for incompleteness, while the legend in the right plot gives the size of the sample after correcting for incompleteness. Having the radial distributions of the more massive MS stars more centrally concentrated than those with lower masses is evidence of mass segregation in the core of 47 Tuc.

follow a linear relation like the one in equation 4.1:

$$log(Mass) = A \times log(R) + B \tag{4.1}$$

As shown in Figure 4.2, we get the following relationships:

$$log(M_{R20}) = -0.83 \times log(R20) + 1.14 \tag{4.2}$$

$$log(M_{R20}) = -0.99 \times log(R50) + 1.71 \tag{4.3}$$

for R20 and R50 respectively. Equations 4.2 and 4.3 are obtained by fitting a linear function

to the three points retrieved from the MS represented by the blue dots in Figure 4.2. The inset accompanying the Figure shows the predicted masses for the bBSS, fBSS, MSBn, RGB and bright and faint WD stars at both R20 and R50. We can see the huge difference between the masses for faint (0.97 and 1.04 $M_{\odot}$) and bright (2.05 and 1.72 $M_{\odot}$) BSS. Table 4.2 shows the values of the masses together with their errors, these are dominated by Poissonian errors. To calculate the errors in our predicted masses, we need the error in R (R20 or R50), using R20 as the example we calculate the errors using the following equation:

$$error(log(R20)) = \pm log(r[N_{R20} \pm \sqrt{N_{R20}}]) \mp log(r[N_{R20}]) \tag{4.4}$$

where $r[N]$ is the radius at the Nth star, for example $r[N_{R20}]$ means the radius at the star where the cumulative distribution reaches 20%. Then the error in the mass is just:

$$error(log(M_{R20})) = m_{R20} \times error(log(R20)) \tag{4.5}$$

where m_{R20} is the slope of the fit for R20. Here we have neglected the errors in the determination of the slope and the determination of the masses for the MS as they are very low and had almost no effect on the final error values.

Looking at the values for the RGB and WDs we can see evidence of mass loss between these two evolutionary stages. To see where this mass loss happens we need the masses of the stages in between the RGB and WD. As we noted before, the HB is contaminated in the UV CMD while the AGB is not identifiable. We then do the same mass prediction exercise limiting the UV field to 105 arcseconds to match the ACS field and taking data from the ACS CMD where possible (normally we would use the matched stars between the two catalogues but as the MS does not extent to faint magnitudes in the ACS data we do not restrict the selection of MS stars to stars measured in all four filters but we do restrain it to the same size field. Same for the WDs). The resulting fits are:

$$log(M_{R20}) = -1.30 \times log(R20) + 1.73 \tag{4.6}$$

$$log(M_{R50}) = -1.74 \times log(R50) + 2.86 \tag{4.7}$$

The results are shown in Figure 4.3, and again the mass values and errors are found in table 4.2.

According to Heyl et al. (2015a), mass loss happens when the star is close to the tip of the AGB. As we mention before, the masses for the RGB and BWD show evidence of mass loss between these stages of evolution. When we include the masses for the HB and AGB we see that this drop in mass happens between the AGB and WDs, but we also see an small increase in the masses between the RGB and AGB that is consistent with the AGBs having

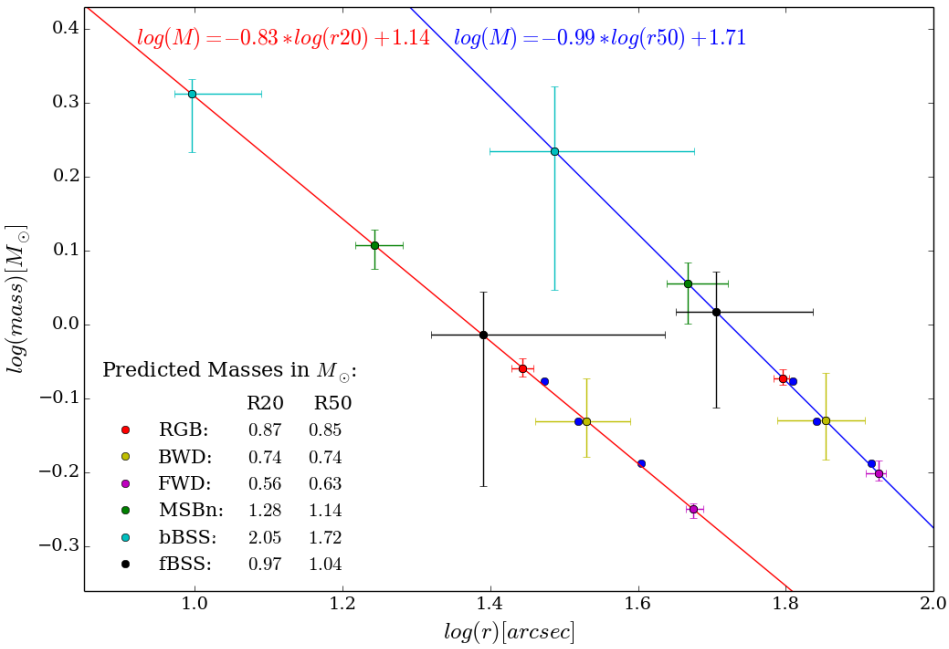

Figure 4.2: Relationship between $log(M)$ and $log(R)$ for R20 (red) and R50 (blue). The equations have been obtained through a linear fit using the known masses for the three regions of the MS (blue dots). The inset shows the predicted masses for the bBSS, fBSS, MSBn, RGB and bright and faint WDs stars at both R20 and R50, the error values can be found in table 4.2.

evolved from slightly more massive stars that ran out of hydrogen earlier than those forming the current RGB. Two other things might explain this behaviour; one, the errors for the masses at this evolved stage are very large and might account for the extra mass; and two, is possible that, even after our efforts to make the HB and AGB as clean as possible, there is still some contamination by evolved BSS.

Another way to test where the mass loss happens is through the cumulative radial distributions. If mass loss does not happen until late in the AGB or is very low before this, then the radial distribution of the upper MS (UMS), RGB, HB, AGB and BWD should be similar. Looking at Figure 4.4 we can see that the distributions of the aforementioned populations look very similar, something that we can confirm through KS-tests which yields p-values over 0.40 for any combination of the four regions and $> 10^{-3}$ for all the samples against the FWD. The detailed results of the KS-tests for the regions selected in Figure 4.4 are presented in table 4.1. Also, if there is mass loss that we could notice between the RGB and HB, then the distribution of the HB should be similar to that of stars of lower masses (not necessarily as low as the

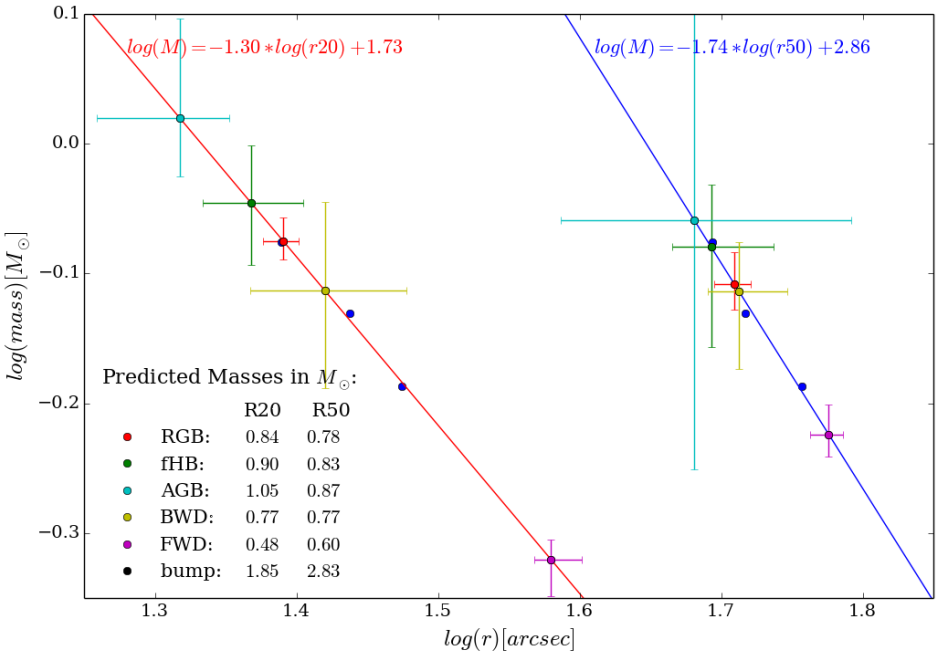

Figure 4.3: Relationship between $log(M)$ and $log(R)$. Similar to Figure 4.2 but with the field reduced to a radius of 105 arcseconds which is the limit for the ACS field. The error values for the masses can also be found in table 4.2.

FWD). Comparing the radial distribution of the HB against the different MS regions used to build the fits for the masses, we confirm that the HB is only related to the UMS, while the difference gets bigger as we go to lower masses with p-values of $\sim 10^{-4}$ for MMS ($0.74M_\odot$) and $\sim 10^{-11}$ for the lower MS (LMS, $0.65M_\odot$) region. Because the HB lasts for a few relaxation times (Heyl et al., 2015b), we can exclude a mass loss of greater than $0.1M_\odot$ on the RGB at nearly the four-sigma level.

Table 4.1: KS-test p-value results between the populations selected on Figure 4.4. The numbers show that every stellar population could have been drawn from the same sample except for the FWD.

					UMS
				RGB	0.91
			HB	0.40	0.41
		AGB	0.98	0.89	0.80
	BWD	0.68	0.60	0.88	0.85
FWD	$\sim 10^{-3}$	$\sim 10^{-3}$	$\sim 10^{-12}$	$\sim 10^{-19}$	$\sim 10^{-28}$

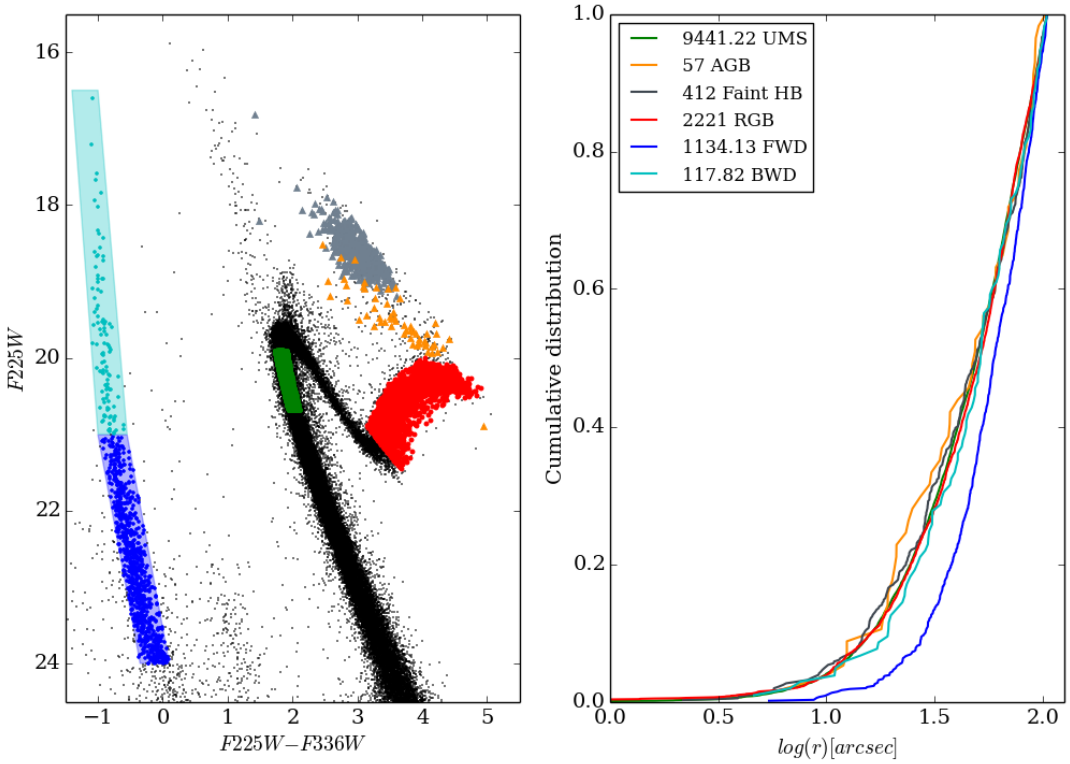

Figure 4.4: CMD (*left panel*) and radial distribution (*right panel*) including 5 evolutionary stages: UMS, RGB, HB, AGB and WD, this last one divided into faint and bright WDs. The selection of the stars for the UMS, RGB and WDs are taken directly from the UV CMD, while the samples for the HB and AGB have been done through the ACS data. In this case, not all the stars have a counter part on the $F606W, F606W - F814W$ CMD as the WDs were not detected with the filters on the visible range. Instead the data was reduced to the same field in order to compare their radial distribution. The colors for the regions on the CMD are the same as in the left plot and specified on the legend.

Table 4.2: Results for the mass prediction in both the WFC3 complete 160 arcseconds field and the reduced ACS field (105 arcseconds). The masses were calculated using equations 4.2, 4.3, 4.6 and 4.7, and the errors with equations 4.4 and 4.5.

	$R \leq 160$				$R \leq 105$			
	M_{R20}	Error	M_{R50}	Error	M_{R20}	Error	M_{R50}	Error
RGB	0.87	+0.03 -0.02	0.85	+0.02 -0.02	0.84	+0.04 -0.03	0.78	+0.04 -0.03
HB	N/A		N/A		0.90	+0.09 -0.09	0.83	+0.09 -0.14
AGB	N/A		N/A		1.05	+0.17 -0.10	0.87	+0.27 -0.31
BWD	0.74	+0.09 -0.08	0.74	+0.10 -0.08	0.77	+0.11 -0.12	0.77	+0.06 -0.10
FWD	0.56	+0.01 -0.01	0.63	+0.02 -0.01	0.48	+0.12 -0.03	0.60	+0.03 -0.02
MSBn	1.28	+0.06 -0.09	1.14	+0.24 -0.13	N/A		N/A	
fBSS	0.97	+0.12 -0.36	1.04	+0.12 -0.27	N/A		N/A	
bBSS	2.05	+0.09 -0.34	1.72	+0.31 -0.60	N/A		N/A	
Bump	N/A		N/A		1.85	+0.43 -0.40	2.83	+1.72 -0.86
BSS	1.78	+0.30 -0.17	1.39	+0.24 -0.20	2.55	+0.39 -0.45	1.73	+0.23 -0.50

Chapter 5

Results

5.1 Blue Stragglers

We have already pointed out the difference between the masses of faint and bright BSS. When looking at the cumulative radial distribution of the two regions of BSS in Figure 5.1 we can also see a significant difference between the two samples. According to the KS-test results, faint and bright BSS are only 1.0% likely to be drawn from the same population and are significantly different from the reference population with p-values of 0.03 for fBSS and $\sim 10^{-6}$ for the bBSS.

Doing a visual examination of the radial distribution plot we noticed a similarity between the fBSS and the MSBn. This is confirmed by the KS-test which yields a p-value of 0.76 suggesting a relation between these two groups of stars that it is not present between the bBSS and MSBn (p-value = 0.01). The KS-test results between the regions highlighted in Figure 5.1 are summarized in table 5.1.

5.2 Evolved Blue Stragglers

Differentiating the various evolutionary stages on the $F225W, F225W - F336W$ CMD after the RGB is complicated. Although the HB seems to be clear, the number of stars and the radial distribution of this branch disagree with the models suggesting an over abundance of

Table 5.1: KS-test p-value results between the populations selected on Figure 5.1.

			bBSS
		fBSS	0.01
	MSBn	0.76	0.01
RGB	$\sim 10^{-5}$	0.03	$\sim 10^{-6}$

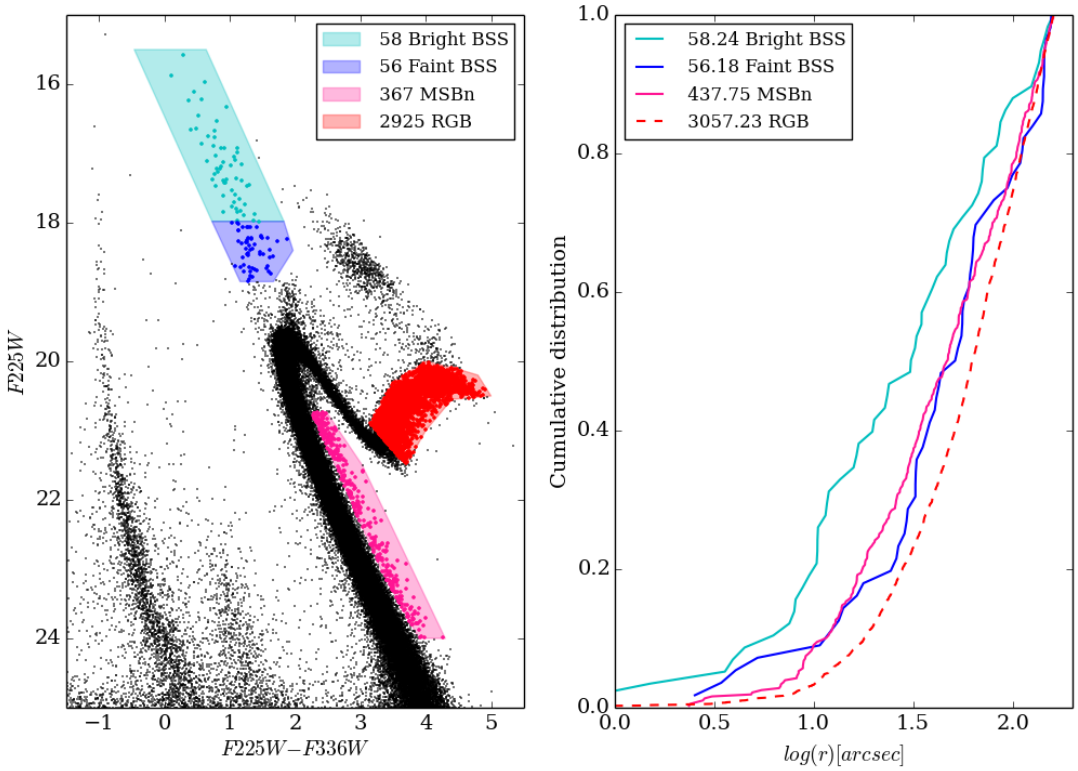

Figure 5.1: *Left:* $F225W, F225W - F336W$ CMD showing the selected stars for the faint and bright BSS, RGB and MSBn. *Right:* Radial distributions for the selected samples. The legend on the CMD has the number of stars before correcting for incompleteness, while the legend on the right plot gives the size of the sample after correcting for incompleteness.

stars. On Figure 5.2, left panel, we can see the upper part of the CMD along with four MESA evolutionary models. The lowest mass model, $0.85M_{\odot}$, shows the evolution for a star with a mass approximately equal to the TO mass. According to this model the RGB lasts for $\sim 4.2 \times 10^8$ years while the HB only $\sim 0.7 \times 10^8$ years. This means that we would expect around 510 HB stars but instead we get a few more than 700. If we do the same exercise but now from the HB to the AGB (15 Myr) we expect an extra 110 stars contaminating the HB, coming to a total of $\sim$ 620 expected stars in this region.

The time scales for the regions outlined on Figure 5.2, along with the numbers for observed and expected stars are presented in table 5.4. Looking at this table, we can see we have included the numbers for the sub-giant branch (SGB). This region, not shown on Figure 5.2 but on the CMD it would extend in the same colour range as the adjacent side of the green region, is included to support our theory that the RGB in these filters is not contaminated by evolved BSS. Doing the calculations to estimate the expected number of stars on the RGB we get a

small difference of only 2.8% with the number of stars observed.

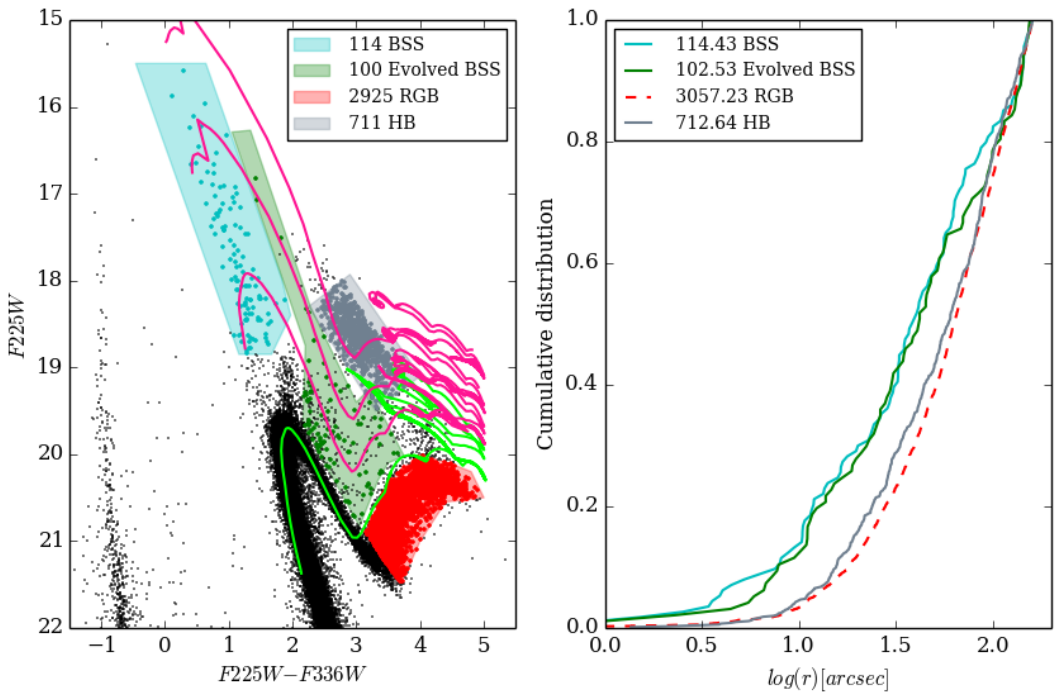

Figure 5.2: *Left:* $F225W, F225W - F336W$ colour-magnitude diagram (CMD), the pink and green curves are MESA evolutionary models for stars with initial masses of $0.85M_{\odot}$, $1.1M_{\odot}$, $1.4M_{\odot}$, and $1.8M_{\odot}$ from bottom to top. *Right:* Radial distributions for the selected samples on the CMD. As on previous figures, the legend on the CMD has the number of stars before correcting for incompleteness, while the legend in the right plot gives the size of the sample after correcting for incompleteness.

Even though we do not see a TO point for the BSS (given that BSS, even of the same mass, can leave the MS at different times depending on the evolutionary stage of the stars that created it), if we follow the path of the models for the BSS of different masses in Figure 5.2, we notice a region between the SGB, RGB, BSS, and HB highlighted in green, where we would expect mainly stars that have evolved from a BSS (because of the likelihood of blends, especially in the region right next to the SGB, we have included a mild error cut in the magnitude of this sample). Calculating the time the $1.4M_{\odot}$ model takes to go from when it leaves the MS to before it reaches the region where the normal stars and the evolved BSS share the same CMD space, and the time it takes the star to evolve from this point up to an AGB star, we get a time of 200 Myr for both sections. Considering these two time scales we would expect a contamination of 100 stars to the HB and surrounding regions.

Looking now at the at the radial distributions for the four coloured regions, the BSS distri-

bution looks similar to that of which we are calling evolved BSS. Table 5.2 shows the p-values obtained from KS-test performed between the different populations. These results support the idea that both distributions, BSS and evolved BSS, were drawn from the same population with a p-value of 0.98. On the other hand, the HB distribution looks visually similar to that of the RGB but the KS-test rejects the hypothesis of these coming from the same distribution with a p-value of $\sim 10^{-3}$. Looking closely we can see that the HB star distribution appears to be slightly more centrally concentrated than the RGB stars. Doing the same for the evolved BSS we can also reject these stars coming from the same sample as the RGB or HB with p-values for the KS-test of 0.01 and 0.03.

To further expand the study and identification of evolved BSS, we now compare our data to photometry obtain from the ACS data. We can see in Figure 5.3 that pointing out the AGB on the ultraviolet CMD is almost impossible, but it becomes much easier on the ACS data, especially at the fainter end of the AGB. By cross-matching the stars from Sarajedini's CMD to ours, we can identify the AGB stars and obtain a cleaner sample for the radial distribution. Again using this smaller data set we see that the number of stars on the HB and AGB are not consistent with the models. According to table 5.5 we expect 370 HB stars but we observe ~ 410, for the AGB the numbers would be 80 and ~ 100 counting the AGB plus the bump highlighted in blue in Figure 5.3. In summary, taking into account the normal evolution of stars, we would expect to observe 450 stars from the HB to the observable part of the AGB but we count 510.

Going back to the evolved BSS, using the MESA models on the ACS CMD, we can now point out where the RGB and HB of the BSS fall on the CMD. The first thing we notice is that the HB for the evolved BSS is brighter than the HB for the normal stars which makes it reasonable to split this population between faint and bright HB. Another interesting result is the fact that the RGB bump for the evolved BSS falls in the same region where the AGB bump was thought to be. This is the reason we have separated this group of stars from the rest of the AGB for further inspection. In this bump alone we count 41 stars. If this is indeed the RGB bump of evolved BSS we would expect to have around 20 stars coming from the evolution of BSS, which means that at least half the stars in this bump are actually evolved BSS and not AGB stars. We must mention that the numbers of expected stars for the $1.8M_{\odot}$ model obtained by starting with a star count of 80 stars on the green region is unrealistic. As we can see on the UV CMD, there are only 4 stars just above the $1.4M_{\odot}$ model, if we take this number as the actual observed count of stars we would expect a total of only 1 and 4 stars for the HB and AGB respectively.

Before splitting the HB and AGB (HB in faint and bright HB, and AGB in AGB and AGB bump) both radial distributions look more centrally concentrated than the RGB. With the samples separated as explained above, we compare the radial distributions for all the populations

highlighted in Figure 5.3 and summarize the results in table 5.3. The bright HB, AGB bump and the BSS distributions look very similar and KS-test results show that we cannot reject the possibility that all three samples are drawn from the same population with p-values of 0.77 for BSS against bright HB and 0.58 for BSS versus AGB bump. Is also important to mention that using the same statistic we can reject the hypothesis that the AGB and the AGB bump are drawn from the same distribution with a p-value of 0.04 and the same for the fHB and bHB with a p-value of 0.08.

For completeness, we can confirm that in this reduced sample the KS-test p-value between the radial distributions of the BSS and the evolved BSS still does not allow us reject the idea that they come from the same population with an even higher result of 0.99. KS-test results also point towards the evolved BSS being related to the bHB and AGB bump with p-values of 0.88 and 0.64 respectively.

Separating the HB and AGB has also help us make more sense of the normal evolution of stars in the cluster. Now the cumulative radial distributions of the RGB, fHB and AGB are more closely related with p-values of 0.40 for RGB vs. fHB, 0.89 for RGB vs. AGB, and 0.98 for fHB vs. AGB.

Table 5.2: KS-test p-value results between the populations selected on Figure 5.2

			BSS
		eBSS	0.98
	RGB	$\sim 10^{-4}$	$\sim 10^{-5}$
HB	$\sim 10^{-3}$	0.03	0.01

Table 5.3: KS-test p-value results between the populations selected on Figure 5.3

						BSS
					eBSS	0.99
				RGB	$\sim 10^{-4}$	$\sim 10^{-5}$
			fHB	0.40	$\sim 10^{-3}$	$\sim 10^{-4}$
		bHB	0.08	0.04	0.88	0.77
	AGB	0.17	0.98	0.89	0.06	0.02
Bump	0.04	0.36	$\sim 10^{-4}$	$\sim 10^{-3}$	0.64	0.58

Table 5.4: Times spent in different regions of the CMD according to the MESA models for the regions selected in Figure 5.2, the evolutionary stage named green makes reference to the green region on the UV CMD refer to as Evolved BSS on the WFC3 CMD. HB for the BSS models ($1.1M_{\odot}$,$1.4M_{\odot}$ and $1.8M_{\odot}$), corresponds to the time the stars spend since the end of the green region until the end of the AGB. The expected number for HB stars from UV CMD counts the stars expected from the HB and AGB.

			Models			
			$0.85M_{\odot}$	$1.1M_{\odot}$	$1.4M_{\odot}$	$1.8M_{\odot}$
SGB	Time (Myr)		415	171	115	54
	WFC3	Obs	2940	N/A		
		Exp	N/A			
Green	Time (Myr)		N/A	319	195	54
	WFC3	Obs	N/A	100		
		Exp	N/A			
RGB	Time (Myr)		420	340	220	84
	WFC3	Obs	3060	N/A		
		Exp	2975	~ 100		
HB+AGB	Time (Myr)		85	182	180	160
	WFC3	Obs	710	N/A		
		Exp	620	~ 100		

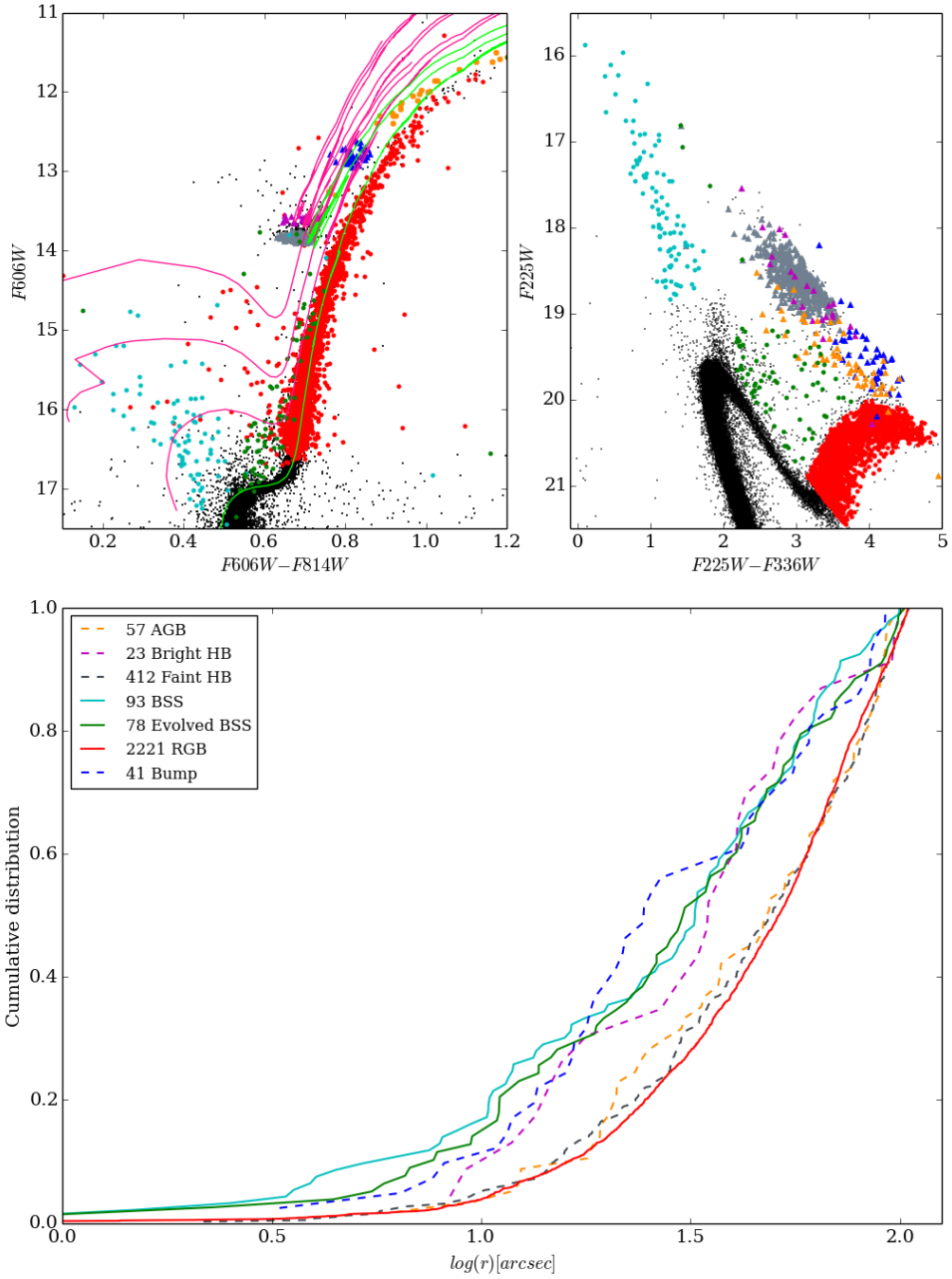

Figure 5.3: *Top-left:* $F606W, F606W - F814W$ $(V, V - I)$ colour-magnitude diagram (CMD) of the core (with $r \leq 105''$) of 47 Tucanae with the same MESA models as Figure 5.2. *Top-right:* $F225W, F225W - F336W$ $(U, U - B)$ CMD for the same region. In both CMDs stars represented by triangles mean they have been selected on the $V, V - I$ CMD, coloured circles on the $U, U - B$. Different colours indicate different populations as indicated on the legend of the bottom plot. *Bottom:* The radial distributions of the different selected evolutionary stages.

Table 5.5: Times spent in different regions of the CMD according to the MESA models for the regions selected from the ACS CMD as shown in Figure 5.3. The green region stars were chosen from the WFC3 data. The count of stars observed on the AGB for the $0.85M_{\odot}$ model includes the stars from the bump highlighted in blue on Figure 5.3. The ages for the AGB on the BSS models ($1.1M_{\odot}$,$1.4M_{\odot}$ and $1.8M_{\odot}$) are calculated within the same magnitude range as the $0.85M_{\odot}$. The numbers for the bump region make reference to the RGB bump from the evolution of normal stars for the $0.85M_{\odot}$ model, while for the BSS models the observed number is the number of stars in the AGB bump. The number of expected stars for the $1.8M_{\odot}$ models are biased by the number of stars in the green region, using the actual number of stars above the $1.4M_{\odot}$ model on the CMD only 1 star on the HB and 4 on the AGB would be expected.

			Models			
			$0.85M_{\odot}$	$1.1M_{\odot}$	$1.4M_{\odot}$	$1.8M_{\odot}$
Green	Time (*Myr*)		N/A	319	195	54
	WFC3	Obs	N/A	80		
		Exp	N/A			
RGB	Time (*Myr*)		420	340	220	84
	ACS	Obs	2200	N/A		
		Exp	N/A	85	90	120
Bump	Time (*Myr*)		35	40	44	20
	ACS	Obs	180	40		
		Exp	185	11	18	28
HB	Time (*Myr*)		70	68	60	51
	ACS	Obs	410	25		
		Exp	370	18	25	72
AGB	Time (*Myr*)		15	15	20	30
	ACS	Obs	100	~ 10		
		Exp	80	~ 8		

Chapter 6

Discussion

6.1 Blue Stragglers

The results reported in section 5.1 indicate there are two distinct BSS sequences present within a radius of 160 arcseconds from the center of 47 Tuc. The p-value of 0.01 obtained for the KS-test between the faint and bright BSS confirms that the two populations have different distributions therefore come from different samples, suggesting different formation mechanisms. Previous studies, including the BSS in the core of 47 Tuc, have also argued in favour of more than one formation mechanisms (Mapelli et al., 2004, 2006; Monkman et al., 2006) going on in this GC; primary stellar evolution and direct collisions. Further more, the estimated masses for faint and bright BSS are also different, with the bright BSS considerably more massive than the faint ones when using R20. The difference in masses become less obvious when we consider R50 especially taking the large errors into account.

The bright BSS are very centrally concentrated (20% of the bright BSS are within 10 arcseconds from the center, and the distribution reaches 50% at only $\sim$ 30 arcseconds) and their cumulative radial distribution does not resemble any of the other populations identifiable on the CMD. This prevents us from linking their formation to an specific group of stars. On the other hand, the mass estimate of $2.05 M_{\odot}$ at R20 for the bright BSS, indicates that they must come from the interactions of at least three stars, possibly through the evolution of hierarchical triple systems or encounters involving more than two stars.

In contrast, the faint BSS are less segregated towards the center but still more concentrated than most of the other populations. Their cumulative radial distribution looks very similar to that of the MSBn (5.1), confirmed by the 0.76 p-value obtained for the KS-test. The resemblance of their radial distributions points to a binary origin for the faint BSS. The estimated masses of these two populations are also similar, with the faint BSS being a little less massive that the MSBn as could be expected for a final product of binary evolution.

6.2 Evolved Blue Stragglers

Before separating the bright and faint HB stars, the combined HB distribution looks more centrally concentrated than that of the RGB, a difference that is sustained by the KS-test results: $\sim 99\%$ probability that the distributions were taken from different samples. According to mass segregation, for a population of stars to be more centrally concentrated would need to be more massive. This fact contradicts the models and theory about stellar evolution where some mass loss is expected between the RGB and HB. Although recent results indicate that the bulk of the mass loss happens when the star is closer to the tip of the AGB (Heyl et al. 2015a, and references within), there is no evidence of mass gain or any other process that could lead to the HB stars being significantly more massive than the RGBs. The models superposed on the CMD in Figure 5.2 show that the HB and AGB of the BSS happens to the right of the normal HB, but there are no stars in that part of the CMD. This is due to saturation of the images in the F336W filter at a magnitude of 15.25, which makes the color of any star with a magnitude above the saturation level pushed below the saturation line, in this case into the same CMD position of the HB for the evolution of normal stars. The contamination to the HB can also be noticed by just counting the stars in that region, which gives an observed number of stars much higher than expected. This overabundance of stars can be justified if we add the expected number of HB stars from normal evolution to the expected number of evolved BSS stars in that part of the CMD by using the time scales derived in section 5.2 (see table 5.4).

The calculation of the number of BSS contaminating the HB was possible through the identification of evolved BSS going though their SGB and beginning of the RGB. The idea came from the fact that there were many stars in a part of the CMD that should not be very populated if we consider stars going through the normal evolution, but once we plotted the BSS models they appear in the right place. The relation of these stars to the BSS was confirmed by their radial distributions with p-value of 0.98 for the KS-test comparing their radial distribution with those of the BSS. Interestingly, when we plot the stars in this green region on the ACS data we find they lie very close to, if not on top of, the SGB and RGB of the evolution of normal stars, close to the portion of the CMD that Beccari et al. (2006) identified to try to find BSS starting their RGB phase. Selecting these stars on the UV CMD allows us to obtain a cleaner sample with a much lower chance of selecting normal RGB stars.

The number of BSS compared to that of the evolved BSS in what we call the green region (see Figure 5.2) suggests a short MS lifetime of $\sim 200 - 300$ Myr. This result disagrees with those found by Sills et al. (2000) and Chatterjee et al. (2013) (between 1 and 3 Gyr). This would be possible considering the formation mechanism dominating in the core are collisions and the MS stars in the core are the more massive ones (i.e. close to the TO), which as we mentioned in section 1.3.2 would leave a BSS with close to the same amount of hydrogen in the core as a TO MS star but with more mass around it speeding up the burning process.

The same overabundance of HB stars is observed when analysing the ACS CMD. In this case when we superpose the models we noticed that the HB for the BSS is brighter than the HB for the normal evolution of stars. In fact, when we split the HB into faint and bright HB, the numbers of observed and expected stars agree. As noted by Beccari et al. (2006), we also find that the distribution of the bright HB and that of the BSS are likely drawn from the same population while the faint HB distribution resembles that of the RGB. Although the result was expected, we have used it to obtained a clean HB sample in the UV CMD that has allowed us to confirm the contamination of the UV HB and the predictions from our models.

From the ACS data, we can see that the overabundance of stars on the HB also extends to the AGB. Again we explained this extra population of stars by adding up the number of expected stars for the AGB and evolved BSS. According to the numbers reported we expect at least half the stars on the AGB plus AGB bump to be evolved BSS. The fact that we can statistically state that the AGB and AGB bump do not come from the same distribution but the BSS and AGB bump most likely do, supports our assumption that this bump is mostly populated by evolved BSS going up the RGB for the first time, more specifically our BSS models place the RGB bump for the BSS in the same region of the AGB bump. Having the radial distribution of the AGB without the bump agreeing with that of the RGB tells us this part of the CMD is dominated by stars coming from the evolution of normal stars. This excess of stars in the AGB was studied earlier by Bailyn (1994) and Beccari et al. (2006), who came to two different conclusions. The first paper suggested that this excess was due to BSS going through their HB stage, but according to our models and as stated in the second paper, the HB of the BSS is much fainter than the AGB bump. Beccari et al., on the other hand, relates this contamination to the *"high-mass binary by-products currently ascending the RGB for the first time"*. Our results are in good agreement with the second paper, but we have also been able to constrain the bulk of the contamination to the AGB bump as due to the RGB bump of the BSS.

Chapter 7

Conclusion

We have identified a large sample of over 200 BSS and evolved BSS in the UV data of the core of 47 Tuc. Expanding our research using available data on the visible range we have studied the properties of this population including their masses, possible formation mechanisms, and their evolution.

When we separate the bright and faint BSS we find that the bright BSS show a much more centrally concentrated radial distribution and higher mass estimates, properties that suggest an origin involving triple or multiple stellar systems. In contrast, the faint BSS are less concentrated, with a radial distribution similar to the MSBn pointing to this populations as their progenitors.

Distinguishing a purely evolved BSS sample from a CMD, had, until now, only been attempted on the HB. The evolved BSS selected on the UV CMD along with the MESA models and the agreement between the radial distributions of the BSS, evolved BSS, bright HB, and AGB bump, allowed us to construct the story of the evolution of BSS. The time scales and number of observed and expected stars agree nicely with the BSS having a post-MS evolution comparable to that of a normal star of the same mass. The disagreement between our estimated MS lifetime and those found by others indicate that a more detailed study of individual BSS properties is necessary to constrain these values.

We have also been able to select clean samples in the different stellar evolutionary stages for the normal evolution of stars. Here we find that the cumulative radial distributions for the upper MS, RGB, faint HB and AGB (without the bump), seem to all come from the same sample as expected for stars of the same mass. It is important to mention that in both the AGB and the AGB bump, we might find stars from the evolution of normal stars as well as those coming from the evolution from BSS, but the number of stars and their radial distributions have allowed us to state the dominant population in each sample.

Future studies using high quality spectra, will tell us more about the formation and evolu-

tion of BSS. Each formation mechanism leaves BSS with different chemical properties and possible companions, both of which could be identified and characterised through spectroscopy.

Bibliography

Ahumada, J. A., & Lapasset, E. 2005, Boletin de la Asociacion Argentina de Astronomia La Plata Argentina, 48, 177 → pages 7

Anderson, A. J. 1997, PhD thesis, University of California, Berkeley → pages 7

Anderson, J., Sarajedini, A., Bedin, L. R., King, I. R., Piotto, G., Reid, I. N., Siegel, M., Majewski, S. R., Paust, N. E. Q., Aparicio, A., Milone, A. P., Chaboyer, B., & Rosenberg, A. 2008, The Astronomical Journal, 135, 2055 → pages 18

Antonini, F., Chatterjee, S., Rodriguez, C. L., Morscher, M., Pattabiraman, B., Kalogera, V., & Rasio, F. A. 2015, ArXiv e-prints, arXiv:1509.05080 → pages 8, 11

Bailyn, C. D. 1994, The Astronomical Journal, 107, 1073 → pages 14, 41

Beccari, G., & Carraro, G. 2015, in Astrophysics and Space Science Library, Volume 413, Ecology of Blue Straggler Stars, ed. H. M. J. Boffin, G. Carraro, & G. Beccari (Springer), 1, doi:10.1007/978-3-662-44434-4_1 → pages 4

Beccari, G., Ferraro, F. R., Lanzoni, B., & Bellazzini, M. 2006, The Astrophysical Journal Letters, 652, L121 → pages 14, 40, 41

Benz, W., & Hills, J. G. 1987, The Astrophysical Journal, 323, 614 → pages 10

Binney, J., & Merrifield, M. 1998, Galactic Astronomy (Princeton University Press) → pages 4

Binney, J., & Tremaine, S. 2008, Galactic Dynamics: Second Edition (Princeton University Press) → pages 5, 6, 7

Boffin, H. M. J., Carraro, G., & Beccari, G. 2015, Ecology of Blue Straggler Stars (Springer), doi:10.1007/978-3-662-44434-4 → pages 8

Bohlin, R. C., & Gilliland, R. L. 2004, The Astronomical Journal, 127, 3508 → pages 16

Bressan, A., Marigo, P., Girardi, L., Salasnich, B., Dal Cero, C., Rubele, S., & Nanni, A. 2012, Monthly Notices of the Royal Astronomical Society, 427, 127 → pages 24

Chatterjee, S., Rasio, F. A., Sills, A., & Glebbeek, E. 2013, The Astrophysical Journal, 777, 106 → pages 11, 40

Chen, Y., Girardi, L., Bressan, A., Marigo, P., Barbieri, M., & Kong, X. 2014, Monthly Notices of the Royal Astronomical Society, 444, 2525 → pages 24

Christensen-Dalsgaard, J. 2015, Monthly Notices of the Royal Astronomical Society, 453, 666 → pages 4

Collins, G. W. I. 1989, The fundamentals of stellar astrophysics (New York: W. H. Freeman and Co.) → pages 2, 4

Davies, M. B. 2015, in Astrophysics and Space Science Library, Volume 413, Ecology of Blue Straggler Stars, ed. H. M. J. Boffin, G. Carraro, & G. Beccari (Springer), 203, doi:10.1007/978-3-662-44434-4_9 → pages 9, 10, 11, 12

de Marchi, F., de Angeli, F., Piotto, G., Carraro, G., & Davies, M. B. 2006, Astronomy & Astrophysics, 459, 489 → pages 7

De Marco, O., Shara, M. M., Zurek, D., Ouellette, J. A., Lanz, T., Saffer, R. A., & Sepinsky, J. F. 2005, The Astrophysical Journal, 632, 894 → pages 8

Fabrycky, D., & Tremaine, S. 2007, The Astrophysical Journal, 669, 1298 → pages 10, 11

Ferraro, F. R., Beccari, G., Rood, R. T., Bellazzini, M., Sills, A., & Sabbi, E. 2004, The Astrophysical Journal, 603, 127 → pages 13, 21

Ferraro, F. R., Sills, A., Rood, R. T., Paltrinieri, B., & Buonanno, R. 2003, The Astrophysical Journal, 588, 464 → pages 21

Ferraro, F. R., Paltrinieri, B., Fusi Pecci, F., Cacciari, C., Dorman, B., Rood, R. T., Buonanno, R., Corsi, C. E., Burgarella, D., & Laget, M. 1997, Astronomy & Astrophysics, 324, 915 → pages 13

Ferraro, F. R., Beccari, G., Dalessandro, E., Lanzoni, B., Sills, A., Rood, R. T., Pecci, F. F., Karakas, A. I., Miocchi, P., & Bovinelli, S. 2009, Nature, 462, 1028 → pages 13

Fiorentino, G., Lanzoni, B., Dalessandro, E., Ferraro, F. R., Bono, G., & Marconi, M. 2014, The Astrophysical Journal, 783, 34 → pages 8

Fiorentino, G., Marconi, M., Bono, G., Dalessandro, E., Ferraro, F. R., Lanzoni, B., Lovisi, L., & Mucciarelli, A. 2015, The Astrophysical Journal, 810, 15 → pages 8

Fregeau, J. M., Cheung, P., Portegies Zwart, S. F., & Rasio, F. A. 2004, Monthly Notices of the Royal Astronomical Society, 352, 1 → pages 11

Fruchter, A., & Sosey, M. 2009, HST MultiDrizzle Handbook (Space Telescope Science Institute) → pages 15

Gilliland, R. L., Bono, G., Edmonds, P. D., Caputo, F., Cassisi, S., Petro, L. D., Saha, A., & Shara, M. M. 1998, The Astrophysical Journal, 507, 818 → pages 8

Harris, W. E. 1996, The Astronomical Journal, 112, 1487, 2010 edition → pages 1, 5, 6, 17

Heggie, D. C. 1975, Monthly Notices of the Royal Astronomical Society, 173, 729 → pages 12

Hesser, J. E., Harris, W. E., & Vandenberg, D. A. 1987, Publications of the Astronomical Society of the Pacific, 99, 1148 → pages 8

Heyl, J., Kalirai, J., Richer, H. B., Marigo, P., Antolini, E., Goldsbury, R., & Parada, J. 2015a, The Astrophysical Journal, 810, 127 → pages iii, 26, 40

Heyl, J., Richer, H. B., Antolini, E., Goldsbury, R., Kalirai, J., Parada, J., & Tremblay, P.-E. 2015b, The Astrophysical Journal, 804, 53 → pages iii, 6, 16, 28

Hilditch, R. W., Howarth, I. D., & Harries, T. J. 2005, Monthly Notices of the Royal Astronomical Society, 357, 304 → pages 17

Hills, J. G., & Day, C. A. 1976, Astrophysical Letters, 17, 87 → pages 10

Hjellming, M. S., & Taam, R. E. 1991, The Astrophysical Journal, 370, 709 → pages 10

Iben, Jr., I., & Tutukov, A. V. 1999, in Astronomical Society of the Pacific Conference Series, Vol. 169, 11th European Workshop on White Dwarfs, ed. S.-E. Solheim & E. G. Meistas, 432 → pages 11

Ivanova, N. 2015, in Astrophysics and Space Science Library, Volume 413, Ecology of Blue Straggler Stars, ed. H. M. J. Boffin, G. Carraro, & G. Beccari (Springer), 179, doi:10.1007/978-3-662-44434-4_8 → pages 9

Kalirai, J. S., Richer, H. B., Anderson, J., Dotter, A., Fahlman, G. G., Hansen, B. M. S., Hurley, J., King, I. R., Reitzel, D., Rich, R. M., Shara, M. M., Stetson, P. B., & Woodley, K. A. 2012, The Astronomical Journal, 143, 11 → pages iii, 15

Kippenhahn, R., & Weigert, A. 1967, Zeitschrift fur Astrophysik, 65, 251 → pages 8

Knigge, C., Gilliland, R. L., Dieball, A., Zurek, D. R., Shara, M. M., & Long, K. S. 2006, The Astrophysical Journal, 641, 281 → pages 14

Knigge, C., Leigh, N., & Sills, A. 2009, Nature, 457, 288 → pages 12

Kozai, Y. 1962, The Astronomical Journal, 67, 591 → pages 11

Lanzoni, B., Dalessandro, E., Perina, S., Ferraro, F. R., Rood, R. T., & Sollima, A. 2007, The Astrophysical Journal, 670, 1065 → pages 13

Leigh, N., Knigge, C., Sills, A., Perets, H. B., Sarajedini, A., & Glebbeek, E. 2013, Monthly Notices of the Royal Astronomical Society, 428, 897 → pages 12

Leonard, P. J. T. 1993, in Bulletin of the American Astronomical Society, Vol. 25, American Astronomical Society Meeting Abstracts, 1329 → pages 11

Lidov, M. L. 1962, Planetary and Space Science, 9, 719 → pages 11

Lombardi, Jr., J. C., Rasio, F. A., & Shapiro, S. L. 1996, The Astrophysical Journal, 468, 797 → pages 10

Mapelli, M., Sigurdsson, S., Colpi, M., Ferraro, F. R., Possenti, A., Rood, R. T., Sills, A., & Beccari, G. 2004, The Astrophysical Journal Letters, 605, L29 → pages 13, 39

Mapelli, M., Sigurdsson, S., Ferraro, F. R., Colpi, M., Possenti, A., & Lanzoni, B. 2006, Monthly Notices of the Royal Astronomical Society, 373, 361 → pages 13, 39

McCrea, W. H. 1964, Monthly Notices of the Royal Astronomical Society, 128, 147 → pages 8

McLaughlin, D. E., Anderson, J., Meylan, G., Gebhardt, K., Pryor, C., Minniti, D., & Phinney, S. 2006, The Astrophysical Journal Supplement Series, 166, 249 → pages 14

Meylan, G. 2000, in Astronomical Society of the Pacific Conference Series, Vol. 211, Massive Stellar Clusters, ed. A. Lançon & C. M. Boily, 215 → pages 5, 7

Milone, A., Piotto, G., Bedin, L. R., King, I. R., Anderson, J., Marino, A. F., Bellini, A., Gratton, R., Renzini, A., Stetson, P. B., Cassisi, S., Aparicio, A., Bragaglia, A., Carretta, E., D'Antona, F., Di Criscienzo, M., Lucatello, S., Monelli, M., & Pietrinferni, A. 2012a, The Astrophysical Journal, 744, 58 → pages 5

Milone, A. P., Piotto, G., Bedin, L. R., & Sarajedini, A. 2008, Memorie della Societ Astronomica Italiana, 79, 623 → pages 12

Milone, A. P., Piotto, G., Bedin, L. R., Aparicio, A., Anderson, J., Sarajedini, A., Marino, A. F., Moretti, A., Davies, M. B., Chaboyer, B., Dotter, A., Hempel, M., Marín-Franch, A., Majewski, S., Paust, N. E. Q., Reid, I. N., Rosenberg, A., & Siegel, M. 2012b, Astronomy & Astrophysics, 540, A16 → pages 12

Monkman, E., Sills, A., Howell, J., Guhathakurta, P., de Angeli, F., & Beccari, G. 2006, The Astrophysical Journal, 650, 195 → pages 13, 39

Naoz, S., & Fabrycky, D. C. 2014, The Astrophysical Journal, 793, 137 → pages 11

Paresce, F., Meylan, G., Shara, M., Baxter, D., & Greenfield, P. 1991, Nature, 352, 297 → pages 13

Paxton, B., Bildsten, L., Dotter, A., Herwig, F., Lesaffre, P., & Timmes, F. 2011, The Astrophysical Journal Supplement Series, 192, 3 → pages 2

Paxton, B., Cantiello, M., Arras, P., Bildsten, L., Brown, E. F., Dotter, A., Mankovich, C., Montgomery, M. H., Stello, D., Timmes, F. X., & Townsend, R. 2013, The Astrophysical Journal Supplement Series, 208, 4 → pages 2

Paxton, B., Marchant, P., Schwab, J., Bauer, E. B., Bildsten, L., Cantiello, M., Dessart, L., Farmer, R., Hu, H., Langer, N., Townsend, R. H. D., Townsley, D. M., & Timmes, F. X. 2015, The Astrophysical Journal Supplement Series, 220, 15 → pages 2

Perets, H. B. 2015, in Astrophysics and Space Science Library, Volume 413, Ecology of Blue Straggler Stars, ed. H. M. J. Boffin, G. Carraro, & G. Beccari (Springer), 251, doi:10.1007/978-3-662-44434-4_11 → pages 8, 9, 10, 11, 12

Perets, H. B., & Fabrycky, D. C. 2009, The Astrophysical Journal, 697, 1048 → pages 10, 11

Piotto, G., De Angeli, F., King, I. R., Djorgovski, S. G., Bono, G., Cassisi, S., Meylan, G., Recio-Blanco, A., Rich, R. M., & Davies, M. B. 2004, The Astrophysical Journal Letters, 604, L109 → pages 12

Pribulla, T., & Rucinski, S. M. 2006, The Astronomical Journal, 131, 2986 → pages 11

Richer, H. B., Heyl, J., Anderson, J., Kalirai, J. S., Shara, M. M., Dotter, A., Fahlman, G. G., & Rich, R. M. 2013, The Astrophysical Journal Letters, 771, L15 → pages 5

Salaris, M., Held, E. V., Ortolani, S., Gullieuszik, M., & Momany, Y. 2007, Astronomy & Astrophysics, 476, 243 → pages 24

Sandage, A. R. 1953, The Astronomical Journal, 58, 61 → pages 1

Sanna, N., Dalessandro, E., Lanzoni, B., Ferraro, F. R., Beccari, G., & Rood, R. T. 2012, Monthly Notices of the Royal Astronomical Society, 422, 1171 → pages 13

Santana, F. A., Muñoz, R. R., Geha, M., Coté, P., Stetson, P., Simon, J., & Djorgovski, S. G. 2012, in Astronomical Society of the Pacific Conference Series, Vol. 458, Galactic Archaeology: Near-Field Cosmology and the Formation of the Milky Way, ed. W. Aoki, M. Ishigaki, T. Suda, T. Tsujimoto, & N. Arimoto, 339 → pages 7

Santucci, R. M., Placco, V. M., Rossi, S., Beers, T. C., Reggiani, H. M., Lee, Y. S., Xue, X.-X., & Carollo, D. 2015, The Astrophysical Journal, 801, 116 → pages 7

Sarajedini, A., Bedin, L. R., Chaboyer, B., Dotter, A., Siegel, M., Anderson, J., Aparicio, A., King, I., Majewski, S., Marín-Franch, A., Piotto, G., Reid, I. N., & Rosenberg, A. 2007, The Astronomical Journal, 133, 1658 → pages 18

Shara, M. M., Saffer, R. A., & Livio, M. 1997, The Astrophysical Journal Letters, 489, L59 → pages 7

Sills, A. 2010, in American Institute of Physics Conference Series, Vol. 1314, American Institute of Physics Conference Series, ed. V. Kalogera & M. van der Sluys, 105–112 → pages 9, 10

Sills, A., Bailyn, C. D., Edmonds, P. D., & Gilliland, R. L. 2000, The Astrophysical Journal, 535, 298 → pages 13, 40

Sills, A., Glebbeek, E., Chatterjee, S., & Rasio, F. A. 2013, The Astrophysical Journal, 777, 105 → pages 12

Sollima, A., Lanzoni, B., Beccari, G., Ferraro, F. R., & Fusi Pecci, F. 2008, The Astrophysical Journal, 481, 701 → pages 12

Sparke, L. S., & Gallagher, III, J. S. 2007, Galaxies in the Universe: An Introduction (Cambridge University Press) → pages 3

Spitzer, L. 1987, Dynamical evolution of globular clusters (Princeton University Press) → pages 6

Stetson, P. 1994, Publications of the Astronomical Society of the Pacific, 106, 250 → pages 16

Stetson, P. B. 1987, Publications of the Astronomical Society of the Pacific, 99, 191 → pages 15

Thompson, I. B., Kaluzny, J., Rucinski, S. M., Krzeminski, W., Pych, W., Dotter, A., & Burley, G. S. 2010, The Astronomical Journal, 139, 329 → pages 8

Tokovinin, A. A. 1997, Astronomy Letters, 23, 727 → pages 11

van den Berg, M., Orosz, J., Verbunt, F., & Stassun, K. 2001, Astronomy & Astrophysics, 375, 375 → pages 11

Ventura, P., Caloi, V., D'Antona, F., Ferguson, J., Milone, A., & Piotto, G. P. 2009, Monthly Notices of the Royal Astronomical Society, 399, 934 → pages 5

Woodley, K. A., Goldsbury, R., Kalirai, J. S., Richer, H. B., Tremblay, P.-E., Anderson, J., Bergeron, P., Dotter, A., Esteves, L., Fahlman, G. G., Hansen, B. M. S., Heyl, J., Hurley, J., Rich, R. M., Shara, M. M., & Stetson, P. B. 2012, The Astronomical Journal, 143, 50 → pages 1, 24